ACS OMEGA

http://pubs.acs.org/journal/acsodf

Article

Clickable Shiga Toxin B Subunit for Drug Delivery in Cancer Therapy

Natalia Danielewicz,[¶] Francesca Rosato,[¶] Jana Tomisch, Jonas Gräber, Birgit Wiltschi, Gerald Striedner, Winfried Römer, and Juergen Mairhofer*

Cite This: *ACS Omega* 2023, 8, 15406−15421

Read Online

ACCESS | Metrics & More | Article Recommendations | Supporting Information

ABSTRACT: In recent years, receptor-mediated drug delivery has gained major attention in the treatment of cancer. The pathogen-derived Shiga Toxin B subunit (STxB) can be used as a carrier that detects the tumor-associated glycosphingolipid globotriaosylceramide (Gb3) receptors. While drug conjugation via lysine or cysteine offers random drug attachment to carriers, click chemistry has the potential to improve the engineering of delivery systems as the site specificity can eliminate interference with the active binding site of tumor ligands. We present the production of recombinant STxB in its wild-type ($STxB_{wt}$) version or incorporating the noncanonical amino acid azido lysine ($STxB_{AzK}$). The $STxB_{wt}$ and $STxB_{AzK}$ were manufactured using a growth-decoupled *Escherichia coli* (*E. coli*)-based expression strain and analyzed via flow cytometry for Gb3 receptor recognition and specificity on two human colorectal adenocarcinoma cell lines—HT-29 and LS-174—characterized by high and low Gb3 abundance, respectively. Furthermore, $STxB_{AzK}$ was clicked to the antineoplastic agent monomethyl auristatin E (MMAE) and evaluated in cell-killing assays for its ability to deliver the drug to Gb3-expressing tumor cells. The $STxB_{AzK}$−MMAE conjugate induced uptake and release of the MMAE drug in Gb3-positive tumor cells, reaching 94% of HT-29 cell elimination at 72 h post-treatment and low nanomolar doses while sparing LS-174 cells. $STxB_{AzK}$ is therefore presented as a well-functioning drug carrier, with a possible application in cancer therapy. This research demonstrates the feasibility of lectin carriers used in delivering drugs to tumor cells, with prospects for improved cancer therapy in terms of straightforward drug attachment and effective cancer cell elimination.

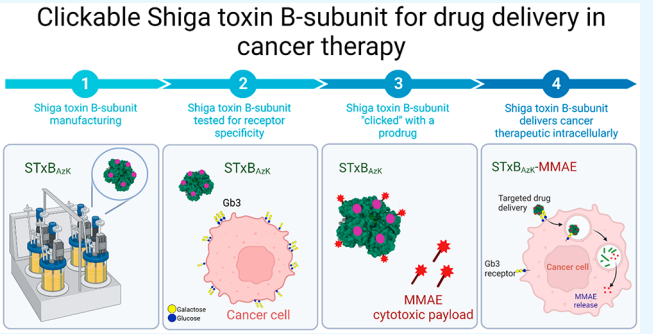

The improvement of strategies for targeted drug delivery has gained importance in multiple fields, e.g., vaccinology, neurology, gene therapy, and cancer treatment.[1−3] A drawback of classically administered therapeutics is their limited capability to navigate across biological barriers to finally reach the intended site of action. Overcoming patient's heterogeneity has been accomplished through precision therapeutics, in which the active pharmaceutical ingredient (API) can be coupled to a carrier capable of recognizing and targeting the cells and tissues of interest with high selectivity (Figure 1). This approach has been investigated to enhance the therapeutic efficacy of treatments by concentrating them at the desired site of action, thus limiting the side effects and dose-related toxicity of a systemic administration. Several new anticancer treatments have shown promising efficacy by exploiting ligands of membrane receptors as selective carriers for a toxic payload.[4,5] Among the most successful drug delivery systems, several antibody−drug conjugates (ADCs), such as Brentuximab Vedotin (cAC10-vcMMAE, SGN-35), have made their appearance on the market and improved the outcome of tumor therapies.[6−8]

The design of an appropriate API delivery system relies, among others, on the type of receptor to be targeted by the carrier of the drug. As such, certain carbohydrate-binding proteins, which recognize sugar moieties attached to proteins and lipids on cell surfaces, offer a wide range of opportunities for the development of carrier-based drug delivery in modern medicine. For example, Shiga Toxin (STx) provides a means for developing novel cancer treatments.[9,10] The STx complex, which is composed of a toxic catalytic A subunit and a pentamer of nontoxic receptor-binding B subunits, has been an effective tool in various therapeutic approaches, including tumor treatment and imaging.[11] If expressed recombinantly without the A subunit, the B subunits are referred to as STxB. STxB is a multipurpose protein applicable, for example, to tumor targeting and vaccine design. Each application is determined by the presence of its preferential receptor, the glycosphingolipid (GSL) globotriaosylceramide (Gb3, also known as CD77 or P^k antigen) on target cells. Upon binding to

Received: February 1, 2023
Accepted: March 10, 2023
Published: April 18, 2023

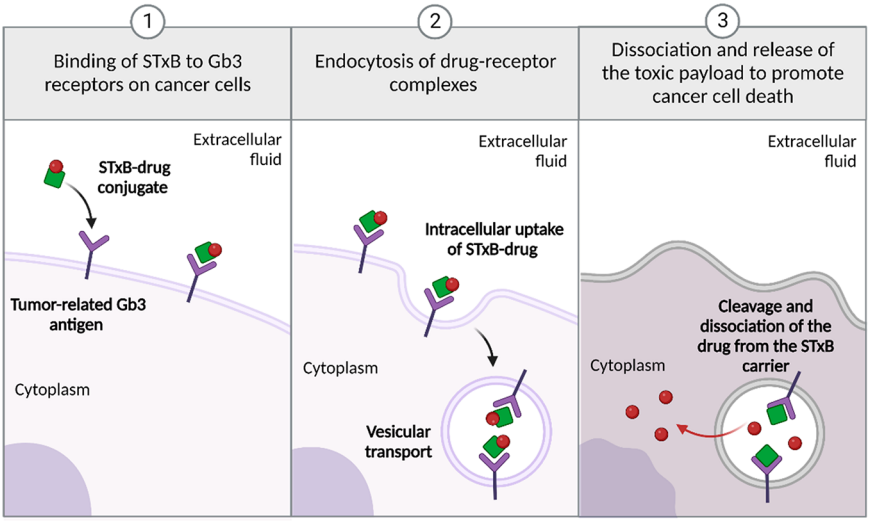

Figure 1. Internalization of Shiga Toxin B subunit (STxB) enabling a method for drug delivery. Created with BioRender.com.

Gb3 at the plasma membrane, STxB is internalized by endocytosis and can be found in clathrin-coated pits.[12] Alternatively, when clathrin-dependent uptake is blocked, STxB endocytosis continues via the clathrin-independent pathway, without the help of the cytosolic machinery. STxB can induce the formation of the STxB-Gb3 cluster domains, imposing negative curvature on the host membrane and promoting lipid reorganization in tubular membrane invaginations.[13,14] These events ultimately lead to STxB entry in the intracellular space and its retrograde transport from early endosomes to the *trans*-Golgi network and the endoplasmic reticulum (ER).[15,16] STxB has been described as a well-performing API carrier if modified via random *N*-hydroxysuccinimide (NHS)−biotin coupling and maleimide chemistry or expressed recombinantly with other fusion proteins and as such enables the delivery of small molecules, modified proteins, or nanoparticles (Figure 1).[17,18] Such methods, however, often require time-consuming optimization experiments, resulting in high batch-to-batch variability, and extensive losses during purification. Alternatively, the site-specific incorporation of reactive noncanonical amino acids (ncAAs) like L-azido lysine (AzK, *N*6-((2-azidoethoxy)-carbonyl)-L-lysine) can be used to overcome the above-mentioned problems and reach higher efficiency of STxB−drug conjugation.[19] This approach can be advanced even further if combined with controlled decoupling of recombinant protein production from cell growth to considerably increase the ncAA incorporation.[20] The enGenes-X-press *E. coli* strains have previously proven to be successful in the production of homologous cholera toxins.[21]

To investigate the efficiency of the selected carrier STxB in drug delivery, the choice of a model drug also plays a crucial role. The most straightforward approach is the selection of previously tested small molecules that are equipped with a cleavable linker. An example of such a drug is DBCO-PEG4-Val-Cit-PAB-MMAE, a toxic payload composed of (I) a potent tubulin polymerization inhibitor, monomethyl auristatin E (MMAE), (II) a reactive dibenzocyclooctyne group (DBCO) that allows copper-free click chemistry to azide groups ($-N_3$; AzK), (III) distanced by a four-unit polyethylene glycol (PEG), and (IV) an enzymatically cleavable linker (Val-Cit-PAB). The peptide bond between Cit-PAB of dipeptide linkers containing valine (Val)-citrulline (Cit) and *p*-amino benzyl alcohol (PAB) is cleaved by a ubiquitous cysteine protease, the cathepsin B, which is located in late endosomes and lysosomes.[22−24] The linker between the cytotoxic drug and the carrier is a critical part of the design of a carrier−drug conjugate, as it must retain stability in the circulation and prevent nonspecific drug release while enabling the detachment of the drug at the site of action.[25,26] The DBCO-PEG4-Val-Cit-PAB-MMAE delivered to lysosomes is cleaved off as PAB-MMAE and released to the cytosol, resulting in mitotic arrest and apoptosis.[27] DBCO-PEG4-Val-Cit-PAB-MMAE has been used for the synthesis of antibody−drug conjugates (ADCs).[28−31] Similar approaches were further proven successful in the literature.[19,32]

Antibodies generally differ as carriers of drugs from STxB by following mainly the lysosomal pathway.[9] STxB is rapidly internalized into target cells by endocytosis,[12,13] and its intracellular sorting is directed by the presence of Gb3 in lipid rafts. Lipid rafts are dynamic membrane microdomains enriched in sphingomyelin and cholesterol.[33] When bound to nonlipid raft Gb3, STxB follows the degradative pathway to lysosomes.[34,35] This fraction of lysosomal STxB offers an opportunity for the targeted intracellular delivery of drugs such as DBCO-PEG4-Val-Cit-PAB-MMAE. The delivery of antitumoral drugs by STxB was previously tested on Gb3-expressing tumor cell lines derived from colorectal, lung, or breast carcinomas.[36−41] These human cell lines are an effective model for assessing the ability of STxB to deliver various treatments *in vitro*.

Here, we tested our products for purity, activity, and intracellular uptake in the Gb3-positive ($Gb3^+$) human colorectal adenocarcinoma cell line HT-29. The specificity of generated STxB variants was further monitored on the LS-174 cell line, derived from human colon adenocarcinoma as well but characterized by a low Gb3 abundance.[42] We customized the STxB carrier with reactive bioorthogonal ("click") handles by the site-specific incorporation of the reactive ncAA AzK. The AzK residue was incorporated in the STxB sequence following three primary requirements: (i) incorporation of the ncAA should occur at the surface of the protein; (ii) the ncAA should be inserted at a distance from the receptor binding site, to avoid interference with the binding; and (iii) the residues in

https://doi.org/10.1021/acsomega.3c00667
ACS Omega 2023, 8, 15406−15421

the pentameric structure should be located at a distance from each other to facilitate their derivatization with the API. In the STxB amino acid sequence, the K9 residue, oriented such that it opposes the Gb3-binding pockets facing the membrane, was chosen to fulfill these conditions. The azido-functionalized proteins are cross-linked by linker molecules carrying compatible reactive groups for click chemistry, such as DBCO. The nontoxic $STxB_{wt/AzK}$ variants were produced using the growth-decoupled *E. coli* enGenes-X-press system[20,21,43] equipped with an orthogonal aminoacyl-tRNA synthetase/amber suppressor tRNA pair,[20] which allows for site-specific ncAA incorporation. The goal is to enable the production of well-defined, site-specifically labeled API carriers to be used for targeted drug delivery in a model *in vitro* setup in which DBCO-PEG4-Val-Cit-PAB-MMAE represents the drug of choice.

MATERIAL AND METHODS

Antibodies and Chemicals. The following antibodies were used: Alexa Fluor 647-labeled anti-6-His epitope tag (Cat. No. 362611) from BioLegend (San Diego, CA, USA), Anti-Giantin mouse monoclonal antibody (Cat. No. ab37266) purchased from Abcam (Waltham, Boston, USA), LAMP1 (D2D11) XP rabbit monoclonal antibody (Cat. No. 9091) obtained from Cell Signaling Technology (Danvers, Massachusetts, USA), and Cy3-AffiniPure F(ab')2 Fragment Donkey Anti-Rabbit IgG (H+L) polyclonal antibody (Cat. No. 711-166-152) and Cy3-AffiniPure Donkey Anti-Mouse IgG (H+L) polyclonal antibody (Cat. No. 715-165-150) supplied by Jackson ImmunoResearch (West Grove, Pennsylvania, USA). The following reagents were obtained from commercial sources: PBS, FBS, HEPES, NEAA, and 0.05% Trypsin-EDTA (1x) were purchased from Gibco (Thermo Fisher Scientific Inc., Rockford, IL, USA). DMSO, penicillin/streptomycin, BSA, DAPI, glycerol, methanol, Triton X-100, and sodium hydrogen carbonate were obtained from Carl Roth GmbH & Co. KG (Karlsruhe, Baden-Württemberg, Germany). D-Luciferin Firefly was provided by Biosynth (Staad, Switzerland), and DMEM (with: 1.0 g/L of glucose, stable glutamine, sodium pyruvate, 3.7 g/L of $NaHCO_3$) was purchased from PAN Biotech (Aidenbach, Bayern, Germany). DL-Threo-1-phenyl-2-palmitoylamino-3-morpholino-1-propanol (PPMP) was obtained from Sigma-Aldrich Chemie GmbH (Saint Louis, MO, USA).

$STxB_{wt/AzK}$ Construct Design. The amino acid sequence of $STxB_{wt}$ protein with a fused C-terminal 6x His-tag was subcloned into pET30a-Cer and[21] and pSCS-T7 × 31[20], and $STxB_{AzK}$ including a C-terminal 6x His-tag with a mutation on position Lys9 in pSCS_T7 × 31 (Supporting Information Figure 1) was used for expression.[44] The three plasmids were named pET30a<$STxB_{wt}$>Cer, pSCS-T7 × 31<$STxB_{wt}$>, and pSCS-T7 × 31<$STxB_{AzK}$>. All materials used for cloning were purchased from New England Biolabs, Frankfurt, Germany (cloning kits), and IDT, Leuven, Belgium (primers and gBLOCKs).

$STxB_{wt/AzK}$ Expression, Purification, and Off-Line Analytics. The expression of all constructs was carried out in the BL21(DE3) strain and enGenes-X-press strain, called V1,[21] originating from BL21(DE3). For μ-bioreactor cultivations, we used the μ-bioreactor Biolector system, Beckmann Coulter, Germany, and for benchtop fed-batch cultures the Dasgip Parallel Bioreactor System, Eppendorf, Germany. Media composition and standard cultivation protocols are described in ref 21. The full-to-low induction strategy was implemented with IPTG (0.5−0.01 mM; GERBU Biotechnik, Heidelberg, Germany) and/or L-arabinose (100 mM; Sigma-Aldrich, A3256, Saint Louis, Missouri, USA). Arabinose (Ara) was only added to the V1 strain as described in ref 21. Five mM of AzK (Iris Biotech, Marktredwitz, Germany) was added to the μ-bioreactor at the start of culture and to the benchtop bioreactor at the start of feed for strains cultivated for $STxB_{AzK}$ production (both V1 and BL21 (DE3)). All μ-scale cultures were run over 24 h. An amount of 1 mg of cell dry mass (CDM) was harvested and enzymatically lysed, and the product yield was analyzed.[45] The results from μ-scale cultivation were translated to a large scale (benchtop 1 L), and the V1 strain was cultivated to 37 g/L of final CDM. For $STxB_{wt}$ production, two different induction strategies were implemented. The first conventional one was direct pulse induction (0.5 mM IPTG + 100 mM Ara). The second optimized fermentation was a combination of pulse and feed induction calculated to the final volume, called low induction (0.01 mM IPTG + 100 mM Ara), partial induction (0.1 mM IPTG + 100 mM Ara), and full induction/low induction (0.5 mM IPTG + 100 mM Ara). For $STxB_{AzK}$, the full induction condition was supplemented with 5 mM AzK.[44] For all benchtop cultivations, cells were harvested at the end of fermentation and resuspended in 50 mM Na_2HPO_4/NaH_2PO_4, 500 mM NaCl, and 20 mM imidazole (Sigma-Aldrich, Saint Louis, Missouri, USA) at pH 7.4 to yield a 30 g CD mg/L suspension. The suspension was homogenized at 700/70 (first stage/second stage) bar for 2 passages on a GEA Niro Soavi PANDAPlus 2000 (GEA, Parma, Italy). Removal of cell debris was achieved by centrifugation and a filtration step on a 0.2 μm sterile filter (Fluorodyne EX EDF, Pall Corporation, Dreieich, Germany). A two-step purification was performed by ÄKTA start (Cytiva, Uppsala, Sweden), starting with HisTrap FF (5 mL) (Cytiva, Uppsala, Sweden) with an immobilized metal affinity chromatography (IMAC) Cytvia protocol followed by size exclusion chromatography (SEC) Superdex 75 10/300 GL with ÄKTA PURE (Cytiva, Uppsala, Sweden). The binding/wash buffer for each purification was: 50 mM Na_2HPO_4/NaH_2PO_4, 500 mM NaCl, and 20 mM Imidazole pH 7.4. The product purified with HisTrap FF was eluted with a binding buffer supplemented with 300 mM imidazole (Sigma-Aldrich, 56749, Vienna, Austria). The SEC purification buffer was phosphate-buffered saline (PBS). The final product was rebuffered in Dulbecco's phosphate-buffered saline buffer (DPBS) (PANtm Biotech, Aidenbach, Germany) using Amicon Ultra Centrifugal Filters (30 kDa cutoff; Darmstadt, Germany).

All off-line analytics like SDS-PAGE and analytical SEC coupled with multiangle light scattering (MALS) were performed as described in ref 21. The molecular weight of the constructs was analyzed by SEC, coupled with right-angle light scattering (RALS), using an OMNISEC RESOLVE/REVEAL combined system (Malvern Panalytical, Malvern, UK). The MS analysis was conducted by directly injecting $STxB_{AzK}$-MMAE into an LC-ESI-MS system (LC: Agilent 1290 Infinity II UPLC, SA, USA). A gradient from 15 to 80% acetonitrile in 0.1% formic acid (using a Waters BioResolve column (2.1 × 5 mm); Vienna, Austria) at a flow rate of 400 μL/min was applied (9 min gradient time). Detection was performed with a Q-TOF instrument (Agilent Series 6230 LC-TOFMS, SA, USA) equipped with the Jetstream ESI source in

https://doi.org/10.1021/acsomega.3c00667
ACS Omega 2023, 8, 15406−15421

positive ion, MS mode (range: 400−3000 Da). Instrument calibration was performed using an ESI calibration mixture (Agilent). Data were processed using MassHunter BioConfirm B.08.00 (Agilent), and the spectrum was deconvoluted by MaxEnt.

$STxB_{wt/AzK}$ Labeling. For cell-based assays, $STxB_{wt}$ and $STxB_{AzK}$ were fluorescently labeled with commercially available dyes. For the initial assessment of Gb3 abundance at the surface of treated cells, commercial STxB (Sigma-Aldrich Chemie GmbH, Germany) was dissolved at 1 mg/mL in PBS and stored at 4 °C prior to its use. For fluorescence labeling, Cy5 monoreactive NHS ester (GE Healthcare, Boston, MA, USA) was used. The fluorescent dye was dissolved at a final concentration of 10 mg/mL in water-free DMSO, aliquoted, and stored at −20 °C before usage according to the manufacturer's protocol. For fluorescence labeling of $STxB_{wt}$ produced in this study, AlexaFluor 647 NHS ester (Thermo Fisher Scientific Inc., Massachusetts, USA) was used. The fluorescent dye was dissolved at a final concentration of 10 mg/mL in water-free DMSO (Carl Roth GmbH & Co. KG, Baden-Württemberg, Germany), aliquoted, and stored at −20 °C before usage according to the manufacturer's protocol. For the labeling reactions, 100 μL of STxB or $STxB_{wt}$ (18 μM) was supplemented with 10 μL of a 1 M $NaHCO_3$ (pH 9) solution so that the molar ratio between dye and STxB was 6:1. The labeling mixture was incubated at 25 °C for 60 min under continuous stirring, and uncoupled dye was removed using Zeba Spin desalting columns (7 kDa MWCO, 0.5 mL, Thermo Fisher Inc., Rockford, IL, USA). Cy5-labeled STxB and AF647-labeled $STxB_{wt}$ were stored at 4 °C and protected from light. $STxB_{AzK}$ (21 μM) was mixed with a ten-times excess of DBCO-AF647 (Jena Bioscience GmbH, Thuringia, Germany) in a total volume of 50 μL in PBS at 22 °C and incubated with shaking at 600 rpm overnight in the dark. 5x SDS reducing buffer was added directly to the sample to stop the reaction. Subsequently, uncoupled dyes were removed using Zeba Spin desalting columns (7 kDa MWCO, 0.5 mL, Thermo Fisher Inc., Rockford, IL, USA). AF647-labeled $STxB_{AzK}$ was stored at 4 °C in the absence of light.

Conjugation of $STxB_{AzK}$ and DBCO-PEG4-Val-Cit-PAB-MMAE. The DBCO-PEG4-Val-Cit-PAB-MMAE from Broadpharm (San Diego, CA, USA) was dissolved in DMSO (Carl Roth GmbH & Co. KG, Baden-Württemberg, Germany) to a final concentration of 5 mM and stored at −20 °C in the dark until use. Cu-free click chemistry (SPAAC) was performed for 16 h at RT in 100 μL of PBS (pH 7.4) containing 21 μM $STxB_{AzK}$ and DBCO-PEG4-Val-Cit-PAB-MMAE at different molar ratios, i.e., 1:5, 1:10, or 1:20. The DMSO concentration was maintained between 8 and 10% (v/v) in the reaction mixtures. To terminate the reaction and remove the unreacted DBCO-PEG4-Val-Cit-PAB-MMAE, 5x SDS reducing buffer was added directly to the reaction mixtures, and the samples were buffer-exchanged with PBS (pH 7.4) using Zeba Spin desalting columns (7 kDa MWCO, 0.5 mL, Thermo Fisher Inc., Rockford, IL, USA). The concentration of the three $STxB_{AzK}$−MMAE conjugates (1:5, 1:10, and 1:20) was measured spectrophotometrically, and the solutions were stored at 4 °C until further use.

Cell Lines. Luciferase-expressing HT-29 and LS-174 human colon adenocarcinoma cell lines (kindly provided by PD Dr. Susana Minguet, Institut für Biologie III, Albert-Ludwigs Universität Freiburg, Germany) were used in this study. Both cell lines were cultured in Dulbecco's Modified Eagle's Medium (DMEM) (with: 1.0 g/L of glucose, stable glutamine, sodium pyruvate, 3.7 g/L of $NaHCO_3$) supplemented with 10% (v/v) heat-inactivated fetal bovine serum (FBS), 2.5 μg/mL of penicillin/streptomycin, 1% (v/v) nonessential amino acids (ncAAs), and 1% (v/v) HEPES, in a humidified incubator with 5% CO_2 at 37 °C. If not stated differently, all experiments were performed in the described complete media.

Depletion of Glucosylceramide-Based Glycosphingolipids by PPMP Treatment. To deplete HT-29 cells of globotriaosylceramide, 2×10^5 cells were seeded in 6-well plates and cultured for 72 h in the presence of 2 μM DL-threo-1-phenyl-2-palmitoylamino-3-morpholino-1-propanol (PPMP), an inhibitor of the synthesis of glucosylceramide-based GSLs.[46] Depletion of Gb3 from the plasma membrane of treated cells was assessed by flow cytometry analysis by using 2.6 nM $STxB_{wt}$ AF647 and $STxB_{AzK}$ AF647 in binding assays.

Ligand- and Cell-Based Binding Assays. The binding of Gb3 to $STxB_{wt/AzK}$ was performed on a MicroCa VP-ITC Isothermal Titration Calorimeter (ITC; MicroCaliTC200, Malvern Panalytical, Malvern, UK) as described in ref 47. For flow cytometry analysis, HT-29 or LS-174 cells were detached from the culture dish with 2 mL of 0.05% trypsin-EDTA (1x) solution for 10 min at 37 °C. Afterward, cells were counted and transferred to a U-bottom 96-well plate (Sarstedt AG & Co. KG, Numbrecht, North Rhine-Westphalia, Germany) to a concentration of 1×10^5 cells/well. To compare the binding of $STxB_{wt}$ AF647 and mutant $STxB_{AzK}$ AF647 to cell surface receptors, cells were incubated with lectins for 30 min on ice, while PBS-treated cells were set as the negative control. Subsequently, cells were centrifuged at 1600*g* for 3 min on ice and washed twice with fluorescence-activated cell sorting (FACS) buffer (PBS supplemented with 3% FBS v/v). When unlabeled $STxB_{wt}$, $STxB_{AzK}$, or $STxB_{AzK}$-DBCO-PEG4-Val-Cit-PAB-MMAE was used, cells were stained with a fluorescently labeled anti-6-His epitope tag Alexa Fluor 647 antibody diluted in FACS buffer to monitor the presence of the lectins at the surface. Incubation was carried out for 20 min on ice and protected from light. At the end of incubation, cells were centrifuged and washed twice as described above. After the last washing step, the cells were resuspended in FACS buffer and transferred to FACS tubes (Kisker Biotech GmbH Co. KG, Steinfurt, North Rhine-Westphalia, Germany). The fluorescence intensity of treated cells was monitored immediately at FACS Gallios (Beckman Coulter Inc., Indianapolis, USA) and further analyzed using FlowJo V.10.5.3 (FlowJo LLC, BD).

Immunofluorescence and Epifluorescence Imaging. Between 5 and 6×10^4 HT-29 cells were seeded on 12 mm glass coverslips in a 4-well plate and allowed to adhere. The next day, cells were stimulated with fluorescently labeled $STxB_{wt}$ AF647 or $STxB_{AzK}$ AF647 (0.13 μM) for 30 min at 4 °C and then washed once with PBS and incubated at 37 °C for the indicated times. Subsequently, cells were fixed with ice-cold methanol for 8 min at −20 °C. Cells were blocked with 3% (w/v) BSA in PBS for 30 min and incubated with target primary antibodies (1:100) for 1 h at RT. After three washes, cells were stained with fluorescently labeled secondary antibodies (1:200) for 30 min at RT in the dark. Nuclei were counterstained with DAPI (5×10^{-9} g/L), and the samples were mounted on coverslips using Mowiol (containing the antibleaching reagent DABCO). Samples were imaged using a Nikon ECLIPSE Ti2 inverted microscope, a 60× oil immersion objective, and a numerical aperture (NA) of 1.40.

https://doi.org/10.1021/acsomega.3c00667
ACS Omega 2023, 8, 15406−15421

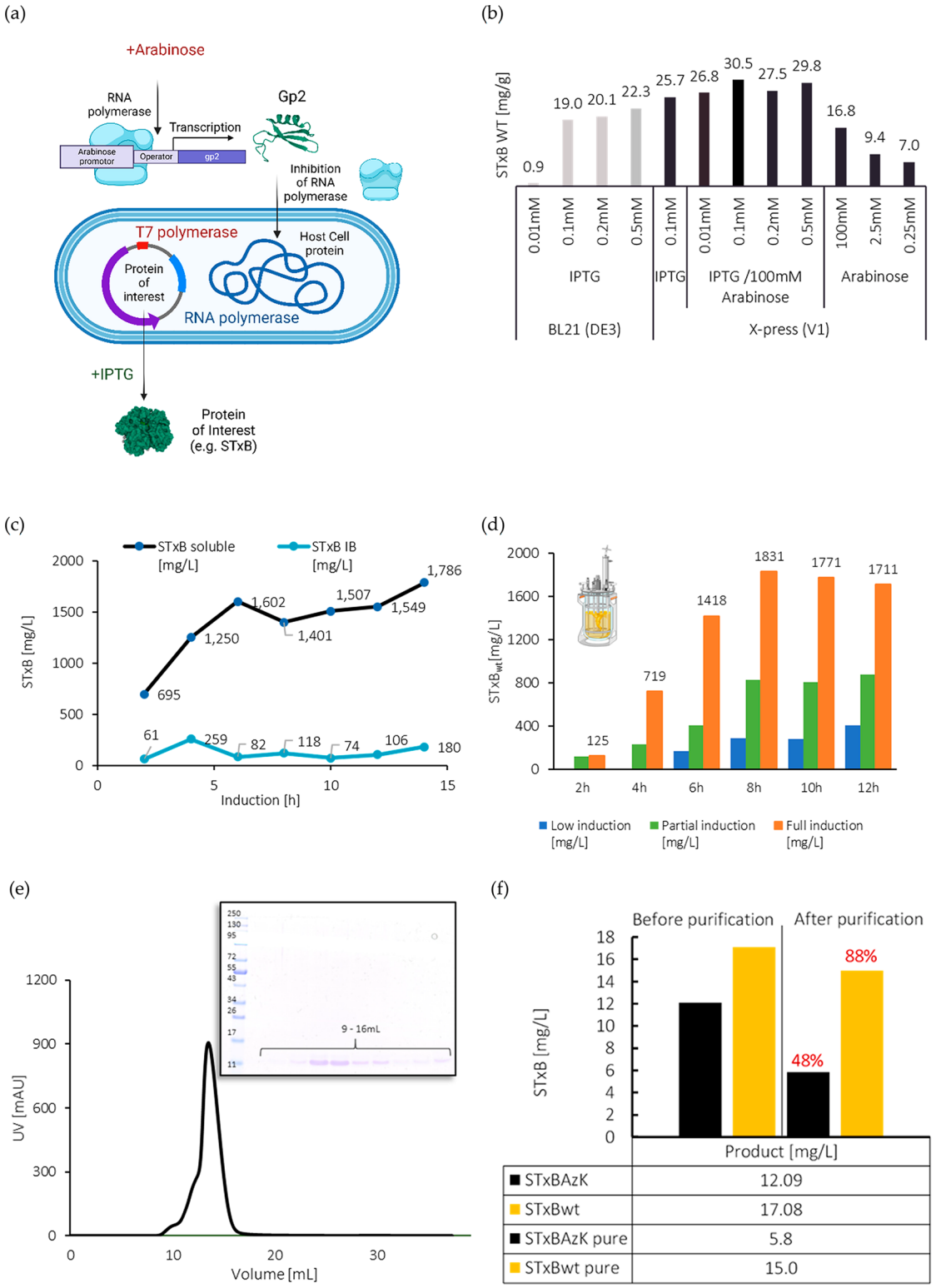

Figure 2. Manufacturing process established with $STxB_{wt}$. (a) enGenes-X-press technology that allows for controlled decoupling of recombinant protein production. (b) Specific yields (mg STxB/g CDM) of STxBwt (pET30a-Cer) production in μ-bioreactor cultivations of the BL21 (DE3) and V1 strains induced at different IPTG (0.01−0.5 mM) and Ara (0.25−100 mM) concentrations. (c) Course of $STxB_{wt}$ (pET30a-Cer) production; volumetric yields (mg/L) of soluble and inclusion body fraction from a 1 L benchtop scale-fed batch process of the V1 strain and pulse induction (0.5 mM IPTG and 100 mM Ara). (d) Volumetric yield (mg/L) of soluble $STxB_{wt}$ (pET30a-Cer) produced in benchtop cultures with V1 with a combination of pulse and feed induction (Ara 100 mM + IPTG low (0.01 mM) or partial (0.1 mM) or full (0.5 mM)). (e) Purification of $STxB_{wt}$ with SEC chromatography (pentamer) and corresponding SDS-PAGE (STxB monomer of 11 kDa). (f) Final yields before versus after purification of $STxB_{AzK}$ (pSCS-T7 × 31) produced using a condition optimized by pET30a<$STxB_{wt}$>Cer plasmid in comparison to pSCS-T7 × 31<$STxB_{wt}$>. The percentage (red) indicates the product remaining after purification. Graphical representation created with BioRender.com.

https://doi.org/10.1021/acsomega.3c00667
ACS Omega 2023, 8, 15406−15421

The images were further analyzed using ImageJ 1.53 from Laboratory for Optical and Computational Instrumentation. A minimum of ≥20 cells per condition were analyzed.

Luciferase-Based Cytotoxicity Assay. For the bioluminescence-based cytotoxicity assay, luciferase-expressing HT-29 and LS-174 tumor cells were counted and plated at a concentration of 1×10^4 cells in 96-well white flat bottom plates in triplicates. The next day, 75 μg/mL of D-firefly luciferin potassium salt was diluted in a complete medium and added to the tumor cells. Bioluminescence (BLI) was measured in the luminometer (Tecan infinity M200 Pro) to establish the BLI baseline. Subsequently, the treatment was added at several concentrations (DBCO-PEG4-Val-Cit-PAB-MMAE: 1 nM, 5 nM, 10 nM; $STxB_{AzK}$: 1.3 nM, 6.5 nM, 26 nM, 52 nM; $STxB_{AzK}$-DBCO-PEG4-Val-Cit-PAB-MMAE: 1.3 nM, 6.5 nM, 26 nM, 52 nM) to the samples, as indicated, and BLI was recorded at several times (24, 48, or 72 h) after incubation at 37 °C. BLI was measured as relative light units (RLUs). RLU signals from tumor cells cultured in the absence of any treatment determine spontaneous cell death. RLU signals from cells treated with 2% Triton X-100 indicate maximal cell death. The percent of specific killings was calculated using the following formula:

$$\%\ \text{of specific killing} = 100 \times (\mathrm{RLU}_{\text{average spontaneous death}} - \mathrm{RLU}_{\text{test}}) / (\mathrm{RLU}_{\text{average spontaneous death}} - \mathrm{RLU}_{\text{average maximal death}})$$

Cell Proliferation (MTT) Assay. To determine IC_{50} values for $STxB_{AzK}$-MMAE, HT-29 or LS-174 cells were treated with increasing concentrations of the $STxB_{AzK}$−drug conjugate for 72 h in a standard MTT assay. An amount of 3×10^4 cells per well was transferred to a 96-well plate with a U-bottom. The cells were centrifuged at 1600*g* for 3 min at RT. The cell pellet was then resuspended in 100 μL of variously concentrated $STxB_{AzK}$-MMAE solutions (1.3, 2.6, 6.5, 13, 19.5, 26, 39, 52, and 65 nM) and transferred to a 96-well flat-bottomed plate. The cells were incubated for 72 h at 37 °C. Subsequently, 10 μL of MTT-labeling solution (MTT Cell Proliferation Kit, Roche) was added to each well, and the cells were incubated for 4 h at 37 °C. Then, 100 μL of the solubilization reagent was added to each well, and the plate was incubated at 37 °C overnight. The next day, the absorbance of the samples was measured at 550 nm using a BioTek microplate reader. The data were further analyzed using GraphPad 6.01 Prism software.

Statistical Analysis. All data in the graphs are presented as mean ± standard deviation (SD) and were calculated from the results of biological experiments. Statistical testing was performed with GraphPad Prism 6.01 software and Microsoft Excel 365 using data of ≥3 biological replicates. Statistical differences in independent, identical samples were determined with a two-tailed, unpaired *t* test. Tests with a *p*-value ≤0.05 are considered statistically significant and marked with an asterisk (*). Nonsignificant results are indicated with ns.

RESULTS AND DISCUSSION

STxB Production and Optimization. To elucidate suitable production conditions for anticipated low-expressing $STxB_{AzK}$, we began the optimization of $STxB_{wt}$ production using a standard expression vector (pET30a-Cer). Our objectives were to implement production process improvements that yield high STxB production before introducing orthogonal pairs (pSCS-T7 × 31 vector) for introducing the AzK inside the STxB amino acid sequence, with production imposing extensive demands on the overall production process of this $STxB_{AzK}$ carrier.

The process development was performed in five steps comprising: (1) optimizing $STxB_{wt}$ production in V1 versus BL21 (DE3) at the μ-scale; (2) upscaling the best performing strain to a 1 L benchtop scale; (3) optimizing the induction condition at the benchtop scale; (4) setting up the purification strategy and stability test for storage; and (5) transferring the manufacturing condition from the $STxB_{wt}$ to $STxB_{AzK}$ variant expressed from the pSCS-T7 × 31 plasmid (Supporting Information Figure 1b).

The V1 strain provided higher quantities of soluble STxB (Figure 2b) and therefore was selected for further production optimization. The addition of arabinose (Ara) upon induction led to transcription and then the translation of a phage-derived protein, called Gp2.[48] This protein is a phage-derived inhibitor of *E. coli* RNA polymerase that stops the V1 strain from further generating biomass. The growth decouples, and the addition of IPTG drives the production of the protein of interest. This resulted in differences in STxB production between wt BL21 (DE3) (22.3 mg/g CDM) which has lower expression capabilities than the V1 strain (29.8 mg/g CDM) at induction with 0.5 mM IPTG (Supporting Information Figure 2a). This corresponded to 189.8 mg/L and 256.4 mg/L, respectively. However, the highest production by V1 was at 0.1 mM IPTG (30.5 mg/g CDM; 269.1 mg/L), where the productivity reaches a plateau (0.1−0.5 mM). Cultures, where V1 was supplemented with Ara only (100−0.25 mM), showed lower expression of $STxB_{wt}$ in comparison to other induction conditions with IPTG supplementation. The V1 strain induced at 0.5 mM IPTG and 100 mM Ara was identified as the best-performing system in μ-scale and subsequently used in all bench-scale cultivations. Additionally, we show the accumulation of $STxB_{wt}$ in soluble and insoluble (IBs) forms over the course of the cultivation (Figure 2c), which was calculated using SDS-PAGE gels under reducing conditions (Supporting Information Figure 2b). It was a pulse induction directly into the production reactor resulting in a 1786 mg/L final yield of soluble $STxB_{wt}$. We estimated that changing the delivery of inducer from pulse to a combination of pulse and feed induction could improve the $STxB_{wt}$ productivity, and therefore we tested low (0.01 mM), partial (0.1 mM), and full induction (0.5 mM) IPTG concentrations introduced steadily by combining feed and pulse induction (Figure 2d). With this approach, we supplemented a steady influx of inducers after the induction time point. This method has proven resourceful for reaching maximal production at 8 h (1831 mg/L).

At the end of fermentation, the harvested, centrifuged, and purified cells (homogenizer and IMAC) were separated with an analytical SEC column. We have observed a characteristic elution peak at 45 kDa (pentamer) that corresponds to the single band (monomer under reducing condition) on SDS-PAGE. This is likely due to polydispersity or hydrodynamic contributions of the STxB molecule, as the asymmetric shape of the peak was only observed with the STxB pentamer when compared to other proteins.[49] As some STxB tends to aggregate, the purity of nonaggregated pentamer was measured and detected at 92% using MALS-SEC (−80 °C storage, Supporting Information Figure 3a). After 2 weeks of storage at 4 °C, the $STxB_{wt}$ started to degrade to 85% purity (Supporting Information Figure 3b); however, a small filtration step could

https://doi.org/10.1021/acsomega.3c00667
ACS Omega 2023, 8, 15406−15421

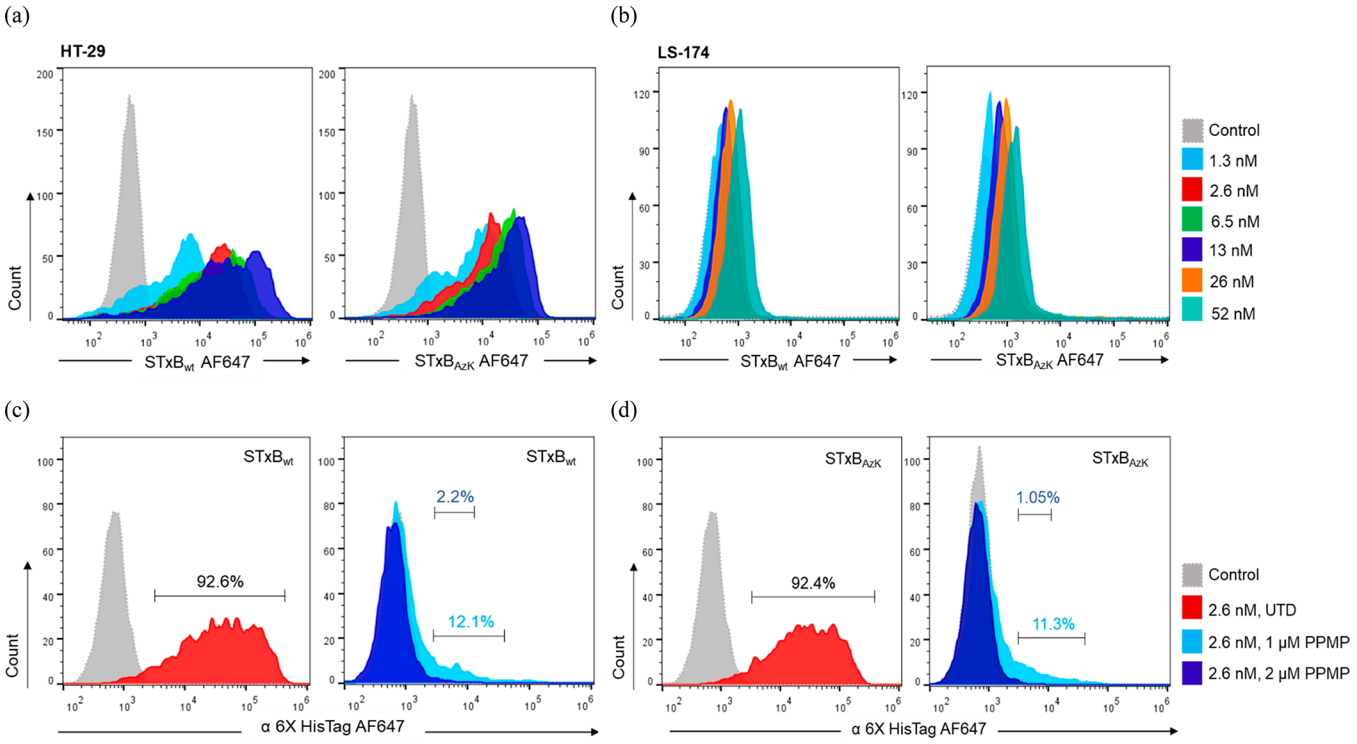

Figure 3. Binding of STxB$_{wt}$ and STxB$_{AzK}$ to HT-29 and LS-174 colon cancer cells. (a) Representative histograms of flow cytometry analysis of gated living HT-29 cells stained with increasing concentrations of fluorescently labeled STxB$_{wt}$ AF647 (left) or STxB$_{AzK}$ AF647 (right) for 30 min on ice. (b) Histograms of fluorescence intensity of gated living LS-174 cells incubated with increasing concentrations of STxB$_{wt}$ AF647 (left) or STxB$_{AzK}$ AF647 (right) for 30 min on ice. (c) Histograms of fluorescence intensity of Gb3^{+} HT-29 cells incubated with 2.6 nM STxB$_{wt}$ in the absence (UTD, left plot) or presence (right panel) of the GLS synthesis inhibitor PPMP. Cells were incubated with STxB$_{wt}$ for 30 min on ice and stained with anti-6-His epitope tag AF647 antibody for 20 min on ice to assess the presence of STxB$_{wt}$ at the surface. At 72 h post-treatment with 1 and 2 μM PPMP, STxB$_{wt}$ no longer binds to HT-29 cells, confirming the depletion of Gb3 from the surface. (d) Histograms of fluorescence intensity of Gb3+ HT-29 cells incubated with 2.6 nM STxB$_{AzK}$, followed by staining with the anti-6-His epitope tag AF647 antibody as described above. Histograms on the left panel show binding of STxB$_{AzK}$ to Gb3 exposed at the surface (UTD) after 30 min incubation on ice. On the right plot, flow cytometry analysis of HT-29 cells pretreated with PPMP for 72 h and incubated with STxB$_{AzK}$ (as indicated before) is illustrated. In the absence of Gb3, the binding of the protein to the plasma membrane is drastically reduced, confirming its specificity toward the Gb3 antigen. The number of cells within the live population (y-axis) is plotted against the fluorescence intensity of the (a, b) STxB$_{wt/AzK}$ AF647 or (c, d) anti-6-His epitope tag AF647. Percentages in (c, d) indicate the number of cells positive for the tested STxB$_{wt/AzK}$.

remove unwanted storage-brought impurities (Supporting Information Figure 3c). Furthermore, storage at −20 °C and −80 °C prevented detectable degradation (data not shown), and repeated defrosting (4-times) from −20 °C storage led to no significant change in purity (Supporting Information Figure 3d). Samples were stored at −20 °C, and storage experiments were supplemented with isothermal titration calorimetry (ITC) prior to carrying out additional experiments (Supporting Information Figure 4). These methods became our quality measurements for testing the biological activity of STxB protein directly after manufacturing and before conducting *in vitro* analysis. This included (1) V1 strain cultivation to 37 g/L CDM and production for 8 h with induction by feed and pulse (0.5 mM IPTG and 100 mM Ara); (2) homogenization, centrifugation, filtration, IMAC, and SEC purification; and (3) storage at −20 °C. The only difference in STxB$_{AzK}$ production was the addition of 5 mM AzK to the feed. The production of STxB$_{AzK}$ produced in pSCS-T7 × 31 was significantly lower (Figure 2f) than STxB$_{wt}$ produced in pET30a-Cer and will require further optimization. Our observation shows that upon purification there is a loss of up to 48% of the final product. This is expected, as the plasmid contains not only the STxB sequence but also the orthogonal pair. The production of coexpressed proteins is more demanding than the single expression carried out by standard pET30a-Cer. We wish to solve this problem by integrating the orthogonal pair in the genome under different strength promoters and ribosome binding sites. With this approach, we will be able to express STxB$_{AzK}$ with the pET30a-Cer vector.

Evaluation of STxB$_{AzK}$ Receptor Recognition and Specificity on Human Colon Cancer Cell Lines HT-29 and LS-174. To monitor the potential of STxB$_{AzK}$ as a carrier for targeted drug delivery, we evaluated its functionality in binding to human colon adenocarcinoma cells. HT-29 and LS-174 are well-characterized cell lines with epithelial morphology and are widely used as preclinical model systems. Moreover, recent studies from Meléndez et al.[42] have described the abundance and species diversity of the Gb3 antigen of HT-29 and LS-174 cells, among other model cancer cell lines. As a result, the amount of Gb3 isoforms was found to be very high in HT-29 cells, while LS-174 displayed low traces of the antigen. In order to confirm the Gb3 abundance at the plasma membrane of these cells, fluorescently labeled STxB-Cy5 from commercial sources was used in flow cytometry assays, further providing a benchmark control (Supporting Information Figure 5).

To assess the capacity of STxB$_{AzK}$ to target the glycosphingolipid Gb3 specifically, we compared its binding

https://doi.org/10.1021/acsomega.3c00667
ACS Omega 2023, 8, 15406−15421

activity to the $STxB_{wt}$ generated in this study. HT-29 and LS-174 cells were screened in flow cytometry analysis to detect the binding of STxB variants (Figure 3). $STxB_{wt}$ was randomly labeled with AlexaFluor 647 NHS ester in a standard reaction. The $STxB_{AzK}$ was conjugated to a DBCO-containing Alexa Fluor 647 probe via SPAAC reaction. Following protein purification, the degree of labeling was estimated spectrophotometrically, and it resulted in the attachment of ∼2.8 and ∼2.1 fluorescent dyes to the $STxB_{wt}$ and $STxB_{AzK}$ pentamers, respectively. HT-29 cells were then stained with four increasing concentrations of $STxB_{wt}$ AF647 or $STxB_{AzK}$ AF647 (1.3, 2.6, 6.5, 13 nM) for 30 min on ice. Then, the unbound STxB was washed away to decrease nonspecific signals, and samples were analyzed via flow cytometry (Figure 3a). The flow cytometry analysis revealed a strong binding of $STxB_{wt}$ (left plot) and $STxB_{AzK}$ (right plot) to $Gb3^+$ HT-29 cells, starting from concentrations in the low nanomolar range. This is visible in a clear shift of the histograms of fluorescence intensity toward higher values. The $STxB_{wt}$ and $STxB_{AzK}$ showed a highly similar, dose-dependent binding pattern to the plasma membrane of cells, suggesting the retained affinity of the STxB mutant toward the Gb3 antigen.

Next, we characterized the binding of $STxB_{wt/AzK}$ to LS-174 cells, which exhibit a low density of the Gb3 antigen at the surface. Figure 3b shows a flow cytometry analysis of LS-174 cells stained with $STxB_{wt}$ AF647 (left plot) or $STxB_{AzK}$ AF647 (right plot). The graphs illustrate the absence of binding by $STxB_{wt/AzK}$ to the plasma membrane for concentrations lower than 10 nM. When higher concentrations of $STxB_{wt/AzK}$ were applied (13−52 nM), a shift of the histograms toward higher values of fluorescence intensity was registered, suggesting a basal presence of Gb3 at the cell surface. The identical binding patterns registered for both protein variants on these two cell lines further support the identity of $STxB_{wt}$ and $STxB_{AzK}$ produced in this study.

To further assess the specificity of $STxB_{AzK}$ toward the tumor-related Gb3 antigen, $Gb3^+$ HT-29 cells were treated with the glucosylceramide synthase (GCS) inhibitor PPMP.[46] PPMP resembles the structure of endogenous ceramide and its product GlcCer and acts as an effective inhibitor of GCS. To this end, GCS is considered a pivotal metabolic target enzyme to clear away ceramides.[50] As a result, PPMP helps sustain a high level of ceramide inside cells by inhibiting its conversion to glucosylated ceramide. To effectively inhibit the synthesis of glucosylceramide-based GSLs and thus deplete Gb3, HT-29 were treated with 1 or 2 μM PPMP for 72 h[44] before flow cytometry analysis. Subsequently, cells were incubated with 2.6 nM $STxB_{wt}$ to confirm the depletion of Gb3 from the plasma membrane. On the left plot of Figure 3c, the typical histogram of binding of $STxB_{wt}$ is visible for untreated cells (UTD). At 72 h post-treatment with 1 μM PPMP, the same concentration of $STxB_{wt}$ (2.6 nM, right plot) did not elicit a notable shift of the histogram toward higher fluorescence intensities, thus revealing a highly reduced binding of $STxB_{wt}$ to the surface of cells. More interestingly, at a concentration of 2 μM PPMP, $STxB_{wt}$ was no longer detected at the membrane of treated cells. $STxB_{wt}$ binding to cancer cells was decreased by more than 90% compared to the untreated control, suggesting a successful depletion of the Gb3 antigen from the plasma membrane. Similarly, the binding of $STxB_{AzK}$, illustrated in Figure 3d, resembles the one observed for $STxB_{wt}$. In the absence of Gb3 at the surface, the AzK variant was no longer able to recognize HT-29 cells (right plot), confirming the exquisite specificity of the generated $STxB_{AzK}$ toward the tumor-associated Gb3 antigen.

These observations are in line with the studies conducted by Rosato et al.[44] The two STxB variants—wild-type and AzK—were compared for their binding specificity and affinity on a panel of Burkitt's lymphoma-derived cells and colon adenocarcinoma cell lines, confirming the specificity of the STxB mutant upon AzK incorporation. The $STxB_{AzK}$ was found to be highly selective for $Gb3^+$ tumor cell lines and successfully targeted them for elimination, while sparing $Gb3^-$ or Gb3-depleted cells.

$STxB_{AzK}$-Mediated Delivery of MMAE to Colon-Derived Cancer Cells and *in Vitro* Tumor Elimination. Given the aberrant expression of several GSLs in cancer, glycan-binding proteins represent a powerful tool for the development of novel targeting strategies. As a proof-of-concept, we have investigated the ability of the generated $STxB_{AzK}$ to deliver the antineoplastic agent MMAE to colon-cancer-derived cell lines by targeting the tumor-related Gb3 antigen. In such a context, STxB represents an optimal carrier with a nanomolar affinity for its receptor, which renders it a suitable vehicle for efficient delivery to target cells. Indeed, the homopentameric STxB can interact with up to 15 Gb3 molecules, with high avidity ($K_d = 10^9\ M^{-1}$).[8,25]

The DBCO-PEG4-Val-Cit-PAB-MMAE (Supporting Information Figure 6) was conjugated to $STxB_{AzK}$ in three different molar ratios (1:5, 1:10, and 1:20) in a standardized SPAAC reaction. The successful attachment of the prodrug to $STxB_{AzK}$ pentamers was confirmed with MS (Supporting Information Figure 7). We evaluated the intracellular accumulation of $STxB_{AzK}$ in HT-29 cells via immunofluorescence studies (Supporting Information Figure 8) and confirmed the ability of the protein to induce its uptake in target cells. Here, the intracellular distribution of $STxB_{wt/AzK}$ was monitored at 3 h after incubation, and lysosomes were stained with antibodies directed against LAMP1 to assess the presence of the STxB in the target compartment. Fluorescence imaging revealed that the $STxB_{AzK}$ variant, similarly to its wild-type counterpart, can be found in the intracellular space of $Gb3^+$ target cells at 3 h postincubation. We registered a limited extent of signal overlap between the carrier and the lysosomes of target cells, highlighted by the arrows in Supporting Information Figure 8b. However, a clear colocalization between $STxB_{AzK}$ and the degradative compartment of HT-29 could not be confirmed. The trafficking route of the $STxB_{wt/AzK}$ within this cell line remains elusive and requires further investigation in the future. Nevertheless, we hypothesized that $STxB_{AzK}$, following its uptake could mediate the specific delivery of DBCO-PEG4-Val-Cit-PAB-MMAE to the intracellular environment of colon-derived cancer cells, ultimately resulting in tumor cell elimination. We cultured $Gb3^+$ HT-29 cells in the presence of DBCO-PEG4-Val-Cit-PAB-MMAE, $STxB_{AzK}$, or the conjugated $STxB_{AzK}$-DBCO-PEG4-Val-Cit-PAB-MMAE (1:10)—referred to as $STxB_{AzK}$-MMAE from now on—for 72 h, and elimination of target cells was recorded as bioluminescence (BLI) at several time points (24, 48, and 72 h). BLI-cytotoxicity assays offer a robust and fast evaluation of the cell viability of luciferase-transduced cell lines, in the presence of specific cytotoxic treatments. For this purpose, HT-29 and LS-174 cells were stably transduced to express luciferase.[44] Since BLI is ATP-dependent, dying cells stop emitting BLI once its remaining intracellular ATP has been used up. Thus, cellular cytotoxicity can be detected as a decrease in BLI.[51,52] Here,

https://doi.org/10.1021/acsomega.3c00667
ACS Omega 2023, 8, 15406−15421

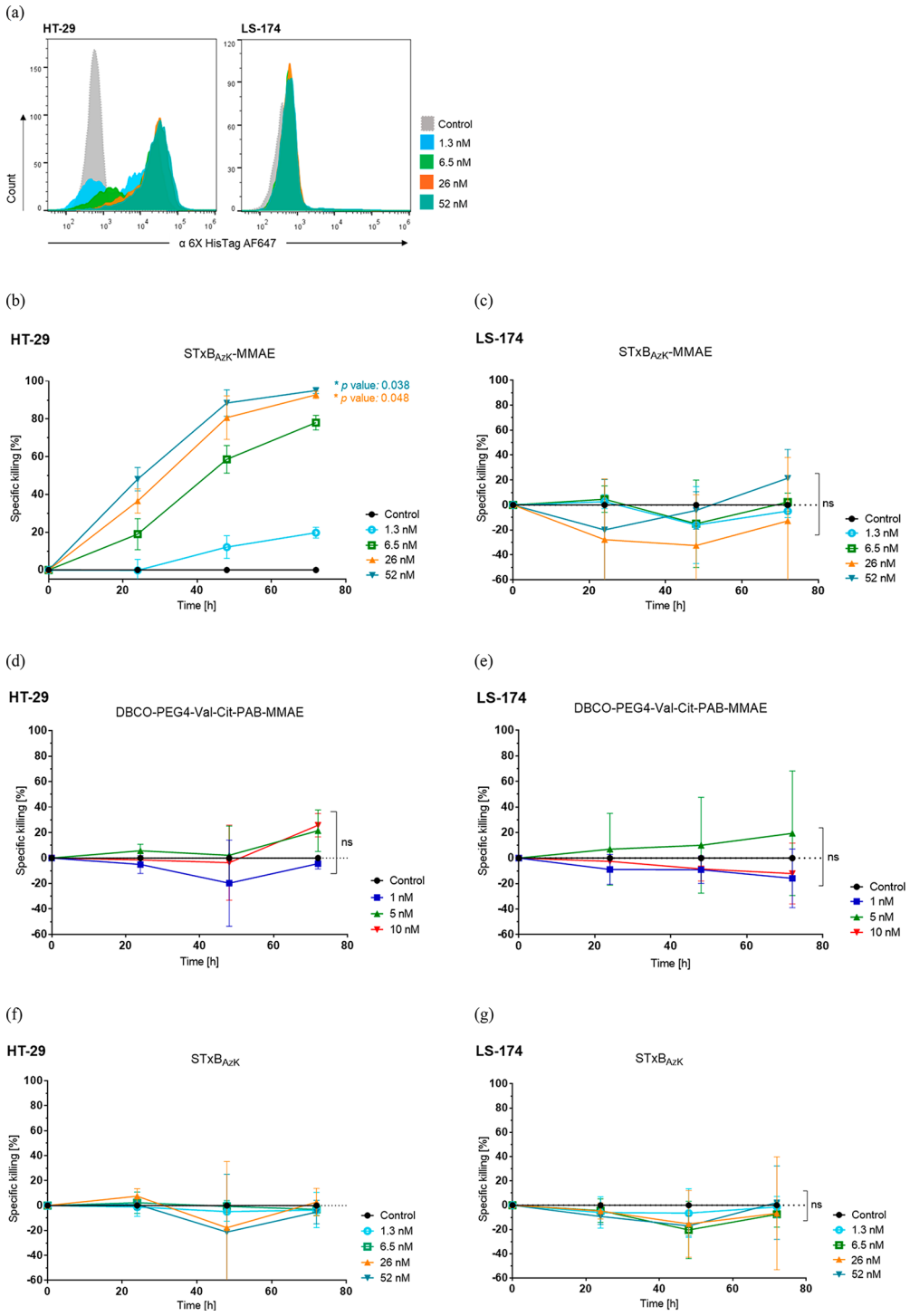

Figure 4. STxB$_{AzK}$-mediated drug delivery to HT-29 and LS-174 tumor cells and *in vitro* specific killing. Tumour cell recognition and quantification of specific killing for HT-29 and LS-174 target cells incubated with STxB$_{AzK}$ after conjugation to MMAE. (a) Representative histograms of flow cytometry analysis of gated living HT-29 cells (left plot) or LS-174 cells (right plot) incubated with increasing concentrations of STxB$_{AzK}$ after attachment of DBCO-PEG4-Val-Cit-PAB-MMAE in a SPAAC reaction (molar ratio 1:10). Cells were incubated with the STxB$_{AzK}$-MMAE conjugate for 30 min on ice, followed by secondary labeling with the anti-6-His epitope tag AF647 antibody for 20 min on ice to detect the presence of STxB$_{AzK}$ at the plasma membrane. The number of cells within the live population (*y*-axis) is plotted against the fluorescence intensity of the anti-6-His epitope tag AF647 (*x*-axis). (b) Cytotoxicity assay of HT-29 cells or (c) LS-174 cells cultured with 1.3, 6.5, 26, or 52 nM STxB$_{AzK}$-MMAE for 72 h. (d) Cytotoxicity assay of HT-29 cells or (e) LS-174 cells cultured with 1, 5, or 10 nM free DBCO-PEG4-Val-Cit-PAB-MMAE for 72 h. (f) Cytotoxicity assay of HT-29 cells or (g) LS-174 cells incubated with unconjugated STxB$_{AzK}$ for 72 h. The percentage of viability was calculated relative to the luminescence from an equal number of input control cells and used to calculate the percentage of specific killing. Results are expressed as a mean ± SD (n = 3) from 3 separate experiments. Statistical differences in independent samples were determined with a two-tailed, unpaired t test for control and treatment groups, at each time point. Tests with a p-value ≤0.05 are considered statistically significant and marked with an asterisk (*). Nonsignificant results are indicated as ns.

https://doi.org/10.1021/acsomega.3c00667
ACS Omega 2023, 8, 15406−15421

(a)

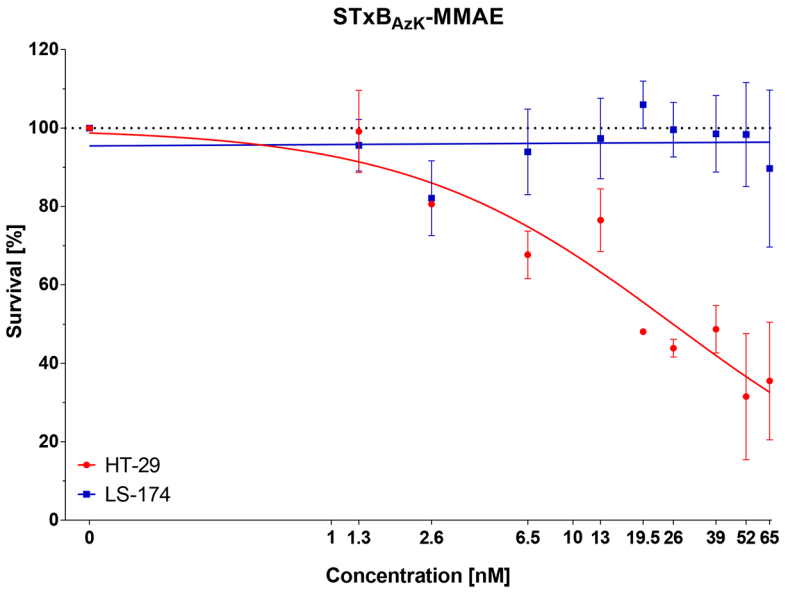

(b)

Cell line	Compound	IC_{50} [nM]
HT-29 ($Gb3^+$)	$StxB_{AzK}$-MMAE	25.89
LS-174 ($Gb3^-$)	$StxB_{AzK}$-MMAE	/

Figure 5. Cytotoxic activity of $STxB_{AzK}$-MMAE on $Gb3^+$ HT-29 and $Gb3^-$ LS-174 tumor cells. (a) Dose-dependent reduction of HT-29 (red) and LS-174 (blue) cell survival following the addition of $STxB_{AzK}$-MMAE in a standard cell proliferation assay (MTT) for 72 h compared to treatment with PBS. Data represent three independent experiments, $n = 3$. (b) IC_{50} values for $STxB_{AzK}$-MMAE efficacy following dose−response cytotoxicity curves presented in (a).

control samples included target cells incubated in the absence of any treatment, counted as spontaneous cell death. Figure 4 presents graphs of *in vitro* killing activity, expressed as a percentage of specific killing induced by the three treatments. Upon conjugation of $STxB_{AzK}$ to DBCO-PEG4-Val-Cit-PAB-MMAE, we first ensured that the attachment of the drug to $STxB_{AzK}$ did not interfere with its binding functionality and receptor recognition. Flow cytometry analysis of $STxB_{AzK}$-MMAE (1:10) revealed a consistent shift in fluorescence intensity upon treatment of cells with the $STxB_{AzK}$−drug conjugate (Figure 4a, left plot). The recognition of Gb3 antigen at the plasma membrane followed a similar pattern to the one reported in Figure 3a, with a dose-dependent binding of $STxB_{AzK}$ to the cell surface. Strikingly, $Gb3^+$ HT-29 cells were efficiently eliminated by the treatment starting from low nanomolar concentrations (Figure 4b). In the presence of the 6.5 nM $STxB_{AzK}$-MMAE conjugate, we recorded ∼50% of specific tumor cells killing at 48 h post-treatment, culminating in 72% of effective tumor cell elimination at 72 h. The higher concentrations (26 and 52 nM) induced cell death at earlier time points, starting from 24 h (approximately 50% cell death) and resulting in nearly complete tumor cell elimination—up to 94%—at 72 h. The $STxB_{AzK}$-MMAE conjugates (1:5) and (1:20) were also investigated for their ability to induce specific killing of HT-29 cells over 72 h of treatment. The activity of the two conjugates in mediating tumor cell death was comparable to the one reported for $STxB_{AzK}$-MMAE (1:10), as illustrated in Supporting Information Figure 9.

To confirm that the observed tumor cell killing was mediated exclusively by the $STxB_{AzK}$−drug conjugates, we further investigated tumor cell cytotoxicity in the presence of 1, 5, or 10 nM free DBCO-PEG4-Val-Cit-PAB-MMAE (Figure 4d). Treatment with the prodrug in the absence of a carrier did not induce the effective killing of tumor cells. At 72 h, we recorded mild cytotoxicity when cells were incubated with 5 nM or 10 nM DBCO-PEG4-Val-Cit-PAB-MMAE, reaching an average of 20% tumor cell death. Similarly, treatment with the $STxB_{AzK}$ carrier alone (1.3, 6.5, 26, or 52 nM) did not induce cell death (Figure 4f). The cells retained viability and exhibited proliferation when coincubated with $STxB_{AzK}$ for 72 h, further confirming the safety of this carrier for biomedical development. Similar studies of STxB-induced cytotoxic activity were also reported by Batisse et al.,[41] who synthesized a series of STxB-MMA conjugates and observed receptor-dependent elimination of $Gb3^+$ HT-29 cells, as opposed to free MMA compounds. The main difference between this conjugation from our approach was that the attachment of a drug requires more steps at harsher chemical reaction conditions. The $STxB_{AzK}$-mediated *in vitro* targeting of tumor cells presented here is significantly relevant and suggests efficient delivery of

https://doi.org/10.1021/acsomega.3c00667
ACS Omega 2023, 8, 15406−15421

the toxic payload to the intracellular environment, along with its correct release.

Moreover, we monitored the specific killing activity of the $STxB_{AzK}$-MMAE conjugate in the presence of a low density of Gb3 antigen on the surface of LS-174 cells. According to the observations previously described (Figure 3b), LS-174 exhibits only a trace amount of this GSL, providing additional control for the specificity of the $STxB_{AzK}$ carrier. Upon attachment of the prodrug to $STxB_{AzK}$, analysis performed in flow cytometry with the $STxB_{AzK}$-MMAE conjugate did not reveal off-target interaction with LS-174 cells nor loss of protein functionality (Figure 4a, right plot). Nevertheless, the binding pattern of $STxB_{AzK}$-MMAE was highly similar to the one described earlier in Figure 3b. For protein concentrations <10 nM, the $STxB_{AzK}$-MMAE conjugate could be detected at the surface of LS-174 cells, as illustrated in the histograms of fluorescence intensity in Figure 4a. At each concentration, a slight but consistent increase in binding to LS-174 cells was registered. The minimal binding of $STxB_{AzK}$-MMAE is reflected in the graph of specific $STxB_{AzK}$-mediated killing reported in Figure 4c. In the same experimental setup, LS-174 cells were incubated with $STxB_{AzK}$-MMAE (1:10) for 72 h, and elimination of target cells was recorded at 24, 48, and 72 h. Control samples included target cells incubated in the absence of treatment and determined spontaneous cell death. In contrast to what we observed for HT-29, LS-174 cells did not show substantial cytotoxicity upon treatment with $STxB_{AzK}$-MMAE. Cells retained their viability, and for doses <10 nM, proliferation was observed. Indeed, cell growth for treated samples was comparable to the negative control and is indicated by the negative values on the *Y*-axis. At the highest dose (52 nM), around 20% of cell cytotoxicity was recorded, accounting for a basal expression of the Gb3 antigen at the plasma membrane. Accordingly, similar observations were collected in cytotoxicity assays of LS-174 cells incubated with the $STxB_{AzK}$-MMAE conjugate (1:5) and (1:20), shown in Supporting Information Figure 10. On the other hand, samples treated with DBCO-PEG4-Val-Cit-PAB-MMAE (1, 5, or 10 nM, Figure 4e) or a $STxB_{AzK}$ carrier (1.3, 6.5, 26, or 52 nM, Figure 4g) did not display consistent cytotoxicity over the 72 h of incubation, further confirming the results reported for HT-29 cells.

The luciferase-killing assay was complemented by a second *in vitro* cytotoxicity assay designed to estimate the half-maximal inhibitory concentration (IC_{50}) of the $STxB_{AzK}$-MMAE conjugate. To this end, a standard colorimetric assay based on the metabolic activity of treated cells was used. The assay relies on the cleavage of tetrazolium salt MTT to form a formazan dye by live cells displaying enzymatic activity, suitable for quantifying cell proliferation and viability. Upon treatment with increasing concentrations of $STxB_{AzK}$-MMAE (1:10) (Figure 5a) for 72 h, the absorbance of treated samples was measured with a spectrophotometer to determine cell viability. The $STxB_{AzK}$-MMAE conjugate (1.3−65 nM) displayed significant cytotoxicity on $Gb3^+$ HT-29 cells, further confirming the results described in Figure 4b. Importantly, $Gb3^-$ LS-174 cells preserved their viability upon incubation with the $STxB_{AzK}$−drug conjugate, indicating once more the specificity of $STxB_{AzK}$ toward the tumor-associated antigen Gb3. According to these results, we determined the IC_{50} for the $STxB_{AzK}$−drug conjugate to define the drug's efficacy. The IC_{50} is a most widely used informative measure of the amount of drug needed to inhibit by half a biological process, represented in this case by tumor cell survival (Figure 5c). The IC_{50} value for $STxB_{AzK}$-MMAE on HT-29 falls in the low nanomolar range (25.89 nM). These results document the efficiency of the Gb3-specific targeting and intracellular delivery using $STxB_{AzK}$ as carrier for the toxic payload.

The data confirm that the receptor-mediated drug delivery system generated in this study enables specific MMAE delivery to Gb3-expressing tumor cells and correct intracellular drug release, while maintaining the drug's cytotoxic activity. On the contrary, the killing activity of the free prodrug DBCO-PEG4-Val-Cit-PAB-MMAE reported in Figure 4d,e was Gb3-independent. The treatment failed to distinguish between target and nontarget cells. LS-174 cells, expressing poor or no Gb3 at the surface, were equally eliminated by the standard MMAE treatment, while their viability was preserved following incubation with $STxB_{AzK}$-MMAE.

CONCLUSIONS

In this work, we have established a platform for the production and *in vitro* analysis of a drug delivery system for $Gb3^+$ colon cancer cells. The $STxB_{AzK}$ mutant was expressed with the pSCS-T7 × 31 plasmid, produced in a 1 L benchtop reactor in fed-batch mode, purified with two-step purification steps and conjugated to the MMAE-containing prodrug DBCO-PEG4-Val-Cit-PAB-MMAE, a precursor of ADCs. The manufacturing of $STxB_{wt}$ (in pET30a-Cer plasmid) was first produced at the highest yield reaching 1786 mg/L after 12 h. The production was improved by changing the conventional pulse induction strategy (0.5 mM pulsated into the reactor) and combining it with induction to the feeding system (0.5 mM divided between feed and reactor). The maximal yield of $STxB_{wt}$ was not only increased to 1831 mg/L but as well achieved 4 h earlier (8 h). This strategy applied to the manufacturing of $STxB_{AzK}$ (pSCS-T7 × 31 plasmid) resulted in much lower yields of 12.09 mg/L due to a more demanding expression platform (coexpression of orthogonal pair). The presence of a unique reactive handle—namely AzK—in $STxB_{AzK}$ enabled the attachment of the prodrug at predefined positions in the STxB pentamer, thereby avoiding interference with its carbohydrate-binding sites. The $STxB_{wt/AzK}$ variants exhibit high specificity for the Gb3 antigen when compared to $Gb3^-$ cells, where no or poor binding was observed. The binding analysis performed with flow cytometry was augmented with a luciferase-based killing assay to quantify the ability of $STxB_{AzK}$ to deliver the antitumoral drug intracellularly. The drug delivery system, $STxB_{AzK}$-DBCO-PEG4-Val-Cit-PAB-MMAE (1:10), successfully crossed the plasma membrane to release the MMAE drug intracellularly and mediated tumor cell death at 72 h with an efficiency as high as 94% and an estimated IC_{50} of 25.89 nM.

Overall, these observations further support the specificity of the generated carrier toward the tumor-related Gb3 antigen and strengthen the hypothesis that $STxB_{AzK}$ is highly efficient in mediating a targeted delivery of antitumoral drugs to cancer cells. Relatively simple click chemistry reactions enable the carrier presented in this study to be conjugated to a toxic payload in a highly selective, site-specific, and efficient manner. Moreover, the toxic moiety in the $STxB_{AzK}$−drug conjugate can be readily exchanged with the purpose of delivering drugs characterized by diverse mechanisms of action. The attachment of drugs to $STxB_{AzK}$ is indeed not limited to small molecules but can be extended to silencing RNAs, peptides, or even antibody fragments. The versatility of this tool is combined to a well-defined control over the drug attachment, as the sites for STxB modification are designed strategically to

https://doi.org/10.1021/acsomega.3c00667
ACS Omega 2023, 8, 15406−15421

be far away from the glycan-binding site, preserving the lectin's specificity toward the antigen of interest.

It is important to mention that the glycosphingolipid Gb3 is also commonly indicated as the Burkitt's lymphoma-associated antigen (BLA), as it is highly expressed on Burkitt's lymphoma (BL) cells.[53] This opens the window for an extended and more comprehensive investigation of the STxB-mediated drug delivery presented here. It would be essentially interesting to evaluate the efficacy of an antitumor treatment based on the $STxB_{AzK}$ carrier targeting the Gb3 antigen on a panel of different human tumor types, including both hematological and solid tumors. This proof-of-concept study could provide significant benefits to the treatment of additional solid tumors, as they have been mostly difficult to target with clinical success. Gb3 overexpression in breast,[54,55] ovarian,[56] and pancreatic[57,58] carcinomas can provide the basis for further application of this tool in the future. Nonetheless, it is of crucial importance to consider that Gb3 is present on the plasma membrane of several nontransformed cells, potentially leading to off-target cytotoxicity upon treatment with $STxB_{AzK}$-MMAE. Moreover, the difference in Gb3 isoforms and abundance among healthy or transformed cells plays a key role in the STxB receptor recognition and could affect the outcome of the therapy.[42,51,59−61] STxB binding and specific intracellular transport within $Gb3^+$ cells are highly influenced by the heterogeneity of Gb3 in terms of chain length, degree of saturation, and hydroxylation of its fatty acyl chain, along with its distribution within lipid rafts of the plasma membrane.[34,62] This structural variability would suggest a screening of target cells to determine the Gb3 heterogeneity before considering such a therapeutic choice.

Further studies to address the stability of $STxB_{AzK}$ conjugates in plasma need to be conducted, to estimate the half-life of the compounds and their sensitivity to catabolism. Moreover, the exact intracellular trafficking route exploited by the carrier in target cells needs to be elucidated to gain a further understanding of the molecular mechanism of action of the $STxB_{AzK}$−drug conjugate. Additionally, while the *in vitro* studies display encouraging properties of the $STxB_{AzK}$−drug model system, *in vivo* mouse tumor models are required to gain further insight into the specific tumor elimination mediated by the $STxB_{AzK}$ carrier.[63,64] The *in vivo* half-life and pharmacokinetic properties of the $STxB_{AzK}$-MMAE conjugate will likely determine if this approach can be successfully employed as a therapeutic. The molecular weight of the conjugate (∼45 kDa) is below the renal excretion threshold, constituting a risk of enhancing its clearance rate, thereby decreasing its therapeutic effect. Nonetheless, the fast kinetics of STxB uptake into target cells has the potential to counteract renal excretion if the treatment is designed for a site-specific application to reach the solid tumor. Additionally, while in the past decades researchers have exploited numerous carbohydrate-binding toxins as drug delivery systems, these carriers are at high risk of eliciting an immune response as a side effect. The clinical success of recombinant immunotoxins (RITs) in patients with a normal immune system is indeed limited by their immunogenicity.[65] Extensive studies of STx functions have highlighted its interaction with antigen presenting cells (APCs), predominantly dendritic cells and macrophages, resulting in APC stimulation and major histocompatibility complex (MHC) classes I and II expression.[66] This is accompanied by the induction of inflammatory cytokine secretion, such as IL-1, IL-6, and TNF-α, by macrophages.[67] The STxB carrier combined to an API might drive the activation of the immune system and the production of neutralizing antibodies (NAbs) by interacting with the Gb3 antigens expressed on APCs and B cells, hampering repeated cycles of treatment and constituting a high risk for the patient. However, STxB-induced activation of dendritic cells results in enhanced $CD8^+$ T cell functionality, which can aid tumor surveillance.[68] The need for balancing the immunogenicity of STxB in tumor therapy becomes evident with the activation of immune cells that can further enhance the antitumor efficacy. Draft Guidance for Industry Assay Development for Immunogenicity Testing of Therapeutic Proteins has recently been published by the US FDA and provide detailed guidelines for a comprehensive evaluation of immunogenicity that should be monitored systematically and on a case-by-case basis.[69] In this case, immunogenicity of the STxB carrier may arise from the presence of nonhuman sequences or epitopes contained in the polypeptide. Moreover, the absence of glycosylation or an altered pattern of glycosylation can expose cryptic B-cell and T-cell epitopes in the protein that cause the protein to appear foreign to the immune system.[70] *In silico* and *in vitro* techniques allow putative B-cell and T-cell epitopes to be identified and eliminated in candidate molecules while maintaining structure and function. An alternative would be to prevent helper T-cell activation by interfering with MHC II presentation or T-cell recognition. As an example, other strategies have also been developed to control the immunogenicity of therapeutic monoclonal antibodies (mAbs) based on increasing the human sequence content and include framework humanization, chimerization, and use of mice with humanized germlines to decrease the rate of NAbs in mice.[71] Other approaches to mitigate the immunogenicity of therapeutic proteins include PEGylation to mask the immunogenic epitopes or combination therapy with immune suppressive molecules that can be toxic and limit the treatment. Each of these strategies could be applied in an attempt to decrease $STxB_{AzK}$ immunogenicity *in vivo*. As a highly critical risk factor, neutralization of cancer treatments by the immune system should be taken into account in the development of STxB−drug conjugates in future steps.

Additionally, as other lectins of different origins have been identified for their selective recognition of the Gb3 antigen,[62] further development in the field of lectin-mediated targeted drug delivery is imaginable. For example, the lectin LecA from *Pseudomonas aeruginosa*[72] or the engineered lectin Mitsuba from *Mytilus galloprovincialis*[34,64] has been already described to successfully target $Gb3^+$ tumor cell lines[42] and offer opportunities for clinical advancement.

In conclusion, these studies showed that the ready-to-click $STxB_{AzK}$ carrier offers the possibility to target glycan epitopes on tumor cells and deliver drugs effective in current cancer therapies, providing an effective appliance for targeted drug delivery in cancer research.

■ ASSOCIATED CONTENT

Data Availability Statement

The data sets generated and/or analyzed during the current study are available from the corresponding authors upon reasonable request.

Supporting Information

The Supporting Information is available free of charge at https://pubs.acs.org/doi/10.1021/acsomega.3c00667.

https://doi.org/10.1021/acsomega.3c00667
ACS Omega 2023, 8, 15406−15421

Supplementary 1: Design of (a) pET30a < $STxB_{wt}$ > Cer, (b) pSCS-T7 × 3 < $STxB_{wt}$ > or pSCS-T7 × 3 < $STxB_{AzK}$>. Supplementary 2: SDS-PAGE gel of $STxB_{wt}$ expression optimization. Supplementary 3: SEC-MALS stability measurement of $STxB_{wt}$. Supplementary 4. ITC measurement of $STxB_{wt/AzK}$ binding to Gb3 receptor. Supplementary 5. Expression of Gb3 antigens at the surface of HT-29 and LS-174 tumor cells. Supplementary 6. Intact protein MS analysis of STxBAzK (8959 Da) and DBCO-PEG4-Cit-PAB-MMAE drug attachment (10615 Da). Supplementary 7. Composition of DBCO-PEG4-Val-Cit-PAB-MMAE toxic payload delivered to Gb3-expressing cancer cells by STxBAzK. Supplementary 8. Fluorescence imaging of HT-29 cells incubated with $STxB_{wt/AzK}$. Supplementary 9. $STxB_{AzK}$-MMAE conjugates (1:5) and (1:20) mediate cytotoxic drug delivery to HT-29 tumor cells and the in vitro-specific killing. Supplementary 9. $STxB_{AzK\text{-}MMAE}$ conjugates (1:5) and (1:20) mediate cytotoxic drug delivery to HT-29 tumor cells and the in vitro-specific killing. Supplementary 10. $STxB_{AzK\text{-}MMAE}$ conjugates (1:5) and (1:20) mediate cytotoxic drug delivery to LS-174 tumor cells and in vitro killing (PDF)

AUTHOR INFORMATION

Corresponding Author

Juergen Mairhofer − *enGenes Biotech GmbH, 1190 Vienna, Austria;* orcid.org/0000-0002-2686-1971; Email: juergen.mairhofer@engenes.cc

Authors

Natalia Danielewicz − *enGenes Biotech GmbH, 1190 Vienna, Austria; Department of Biotechnology, University of Natural Resources and Life Sciences, 1190 Vienna, Austria*

Francesca Rosato − *Faculty of Biology, University of Freiburg, 79104 Freiburg, Germany; Signaling Research Centers BIOSS and CIBSS, University of Freiburg, 79104 Freiburg, Germany*

Jana Tomisch − *Faculty of Biology, University of Freiburg, 79104 Freiburg, Germany; Signaling Research Centers BIOSS and CIBSS, University of Freiburg, 79104 Freiburg, Germany*

Jonas Gräber − *Faculty of Biology, University of Freiburg, 79104 Freiburg, Germany; Signaling Research Centers BIOSS and CIBSS, University of Freiburg, 79104 Freiburg, Germany*

Birgit Wiltschi − *Department of Biotechnology, University of Natural Resources and Life Sciences, 1190 Vienna, Austria; Austrian Centre of Industrial Biotechnology (ACIB), 1190 Vienna, Austria;* orcid.org/0000-0001-5230-0951

Gerald Striedner − *Department of Biotechnology, University of Natural Resources and Life Sciences, 1190 Vienna, Austria*

Winfried Römer − *Faculty of Biology, University of Freiburg, 79104 Freiburg, Germany; Signaling Research Centers BIOSS and CIBSS, University of Freiburg, 79104 Freiburg, Germany; Freiburg Institute for Advanced Studies (FRIAS), University of Freiburg, 79104 Freiburg, Germany*

Complete contact information is available at: https://pubs.acs.org/10.1021/acsomega.3c00667

Author Contributions

Conceptualization of the study, N.D., F.R., W.R., and J.M.; methodology, N.D., F.R., J.T., J.G., G.S., W.R., B.W., and J.M.; formal analysis, N.D., F.R., J.T., and J.G.; investigation, N.D. and F.R.; data curation, N.D., F.R., J.T., and J.G.; writing−original draft preparation, N.D. and F.R.; writing−review and editing, N.D., F.R., B.W., G.S., W.R., and J.M.; supervision, W.R. and J.M.; project administration, J.M.; funding acquisition, J.M. and W.R. All authors have read and agreed to the published version of the manuscript.

Author Contributions

[¶]N.D. and F.R. contributed equally.

Funding

This research was funded by the European Union's Horizon 2020 Research and Innovation Program, under the Marie Skłodowska−Curie grant agreement synBIOcarb (No. 814029). Moreover, W.R. acknowledges support by the Deutsche Forschungsgemeinschaft (DFG, German Research Foundation) under Germany's Excellence Strategy (EXC-2189) and from the Major Research Instrumentation (project number: 438033605) by the Ministry for Science, Research and Arts of the State of Baden-Württemberg (Az: 33-7532.20) and by the Freiburg Institute for Advanced Studies (FRIAS).

Notes

LRS chambers used as blood sources were purchased from the blood bank of the University Medical Centre Freiburg (approval of the University Freiburg Ethics Committee: 147/15).

The authors declare the following competing financial interest(s): Juergen Mairhofer is CEO and CSO of enGenes Biotech, a company providing technology, IP, and fee-for-service in the field of recombinant protein expression.

ACKNOWLEDGMENTS

We thank PD Dr. Susana Minguet from the University of Freiburg, Germany, for providing the luciferase-expressing HT-29 and LS-174 cells used in this study. We also express gratitude to Dr. Pavel Salavei of the CIBSS Signaling Factory, University of Freiburg, Germany, for his help and guidance in flow cytometry. We further thank Rajeev Pasupuleti from the Austrian Centre of Industrial Biotechnology, Graz, Austria, for providing pSCS_T7 × 31 plasmid.

ABBREVIATIONS

ADCs	Antibody−drug conjugates
API	Active pharmaceutical ingredient
AzK	Azido lysine
BLA	Burkitt's lymphoma-associated antigen
BLI	Bioluminescence
DBCO	Dibenzocyclooctyne
DMEM	Dulbecco's modified eagle medium
FACS	Fluorescence-activated cell sorting
FDA	Food and Drug Administration
Gb3	Globotriaosylceramide
GCS	Glucosylceramide synthase
GSL	Glycosphingolipid
IC_{50}	Half-maximal inhibitory concentration
mAbs	Monoclonal antibodies
MMAE	Monomethyl auristatin E
NAbs	Neutralizing antibodies
ncAA	Noncanonical amino acid
PBS	Phosphate-buffered saline

https://doi.org/10.1021/acsomega.3c00667
ACS Omega 2023, 8, 15406−15421

PEG	Polyethylene glycol
PPMP	1-Phenyl-2-palmitoylamino-3-morpholino-1-propanol
RLU	Relative light units
RTIs	Recombinant immunotoxins
SDS-PAGE	Sodium dodecyl sulfate-polyacrylamide gel electrophoresis
SPAAC	Strain-promoted azide−alkyne cycloaddition
STxB	Shiga toxin B subunit
$STxB_{AzK}$	Shiga toxin B subunit azido lysine
$STxB_{wt}$	Shiga toxin B subunit wild-type

REFERENCES

(1) Tiwari, G.; Tiwari, R.; Bannerjee, S.; Bhati, L.; Pandey, S.; Pandey, P.; Sriwastawa, B. Drug Delivery Systems: An Updated Review. *Int. J. Pharm. Investig.* **2012**, *2* (1), 2.

(2) Vargason, A. M.; Anselmo, A. C.; Mitragotri, S. The Evolution of Commercial Drug Delivery Technologies. *Nat. Biomed. Eng.* **2021**, *5* (9), 951−967.

(3) Liu, G.; Yang, L.; Chen, G.; Xu, F.; Yang, F.; Yu, H.; Li, L.; Dong, X.; Han, J.; Cao, C.; Qi, J.; Su, J.; Xu, X.; Li, X.; Li, B. A Review on Drug Delivery System for Tumor Therapy. *Front. Pharmacol.* **2021**, *12*, 1−22.

(4) Majumdar, S.; Siahaan, T. J. Peptide-Mediated Targeted Drug Delivery. *Med. Res. Rev.* **2012**, *32*, 637−658.

(5) Flygare, J. A.; Pillow, T. H.; Aristoff, P. Antibody-Drug Conjugates for the Treatment of Cancer. *Chem. Biol. Drug Des.* **2013**, *81*, 113−121.

(6) Khongorzul, P.; Ling, C. J.; Khan, F. U.; Ihsan, A. U.; Zhang, J. Antibody - Drug Conjugates : A Comprehensive Review. *Mol. Cancer Res.* **2020**, *18* (18), 3−19.

(7) Lambert, J. M.; Chari, R. V. J. Ado-Trastuzumab Emtansine (T-DM1): An Antibody - Drug Conjugate (ADC) for HER2-Positive Breast Cancer. *Am. Chem. Soc.* **2014**, *57*, 6949−6964.

(8) Drago, J. Z.; Modi, S.; Chandarlapaty, S. Unlocking the Potential of Antibody-Drug Conjugates for Cancer Therapy. *Nat. Rev. Clin. Oncol.* **2021**, *18*, 327−344.

(9) Luginbuehl, V.; Meier, N.; Kovar, K.; Rohrer, J. Intracellular Drug Delivery: Potential Usefulness of Engineered Shiga Toxin Subunit B for Targeted Cancer Therapy. *Biotechnol. Adv.* **2018**, *36* (3), 613−623.

(10) Robert, A.; Wiels, J. Shiga Toxins as Antitumor Tools. *Toxins (Basel).* **2021**, *13* (10), 690.

(11) Danielewicz, N.; Rosato, F.; Dai, W.; Römer, W.; Turnbull, W. B.; Mairhofer, J. *Microbial Carbohydrate-Binding Toxins - From Etiology to Biotechnological Application.* **2022**, *59* (April), 107951.

(12) Johannes, L.; Römer, W. Shiga Toxins from Cell Biology to Biomedical Applications. *Nat. Rev. Microbiol.* **2010**, *8* (2), 105−116.

(13) Römer, W.; Berland, L.; Chambon, V.; Gaus, K.; Windschiegl, B.; Tenza, D.; Aly, M. R. E.; Fraisier, V.; Florent, J. C.; Perrais, D.; Lamaze, C.; Raposo, G.; Steinem, C.; Sens, P.; Bassereau, P.; Johannes, L. Shiga Toxin Induces Tubular Membrane Invaginations for Its Uptake into Cells. *Nature* **2007**, *450* (7170), 670−675.

(14) Windschiegl, B.; Orth, A.; Romer, W.; Berland, L.; Stechmann, B.; Bassereau, P.; Johannes, L.; Steinem, C. Lipid Reorganization Induced by Shiga Toxin Clustering on Planar Membranes. *PLoS One* **2009**, *4* (7), 1−11.

(15) Mallard, F.; Antony, C.; Tenza, D.; Salamero, J.; Goud, B.; Johannes, L. Direct Pathway from Early/Recycling Endosomes to the Golgi Apparatus Revealed through the Study of Shiga Toxin B-Fragment Transport. *J. Cell Biol.* **1998**, *143* (4), 973−990.

(16) Sandvig, K.; Kavaliauskiene, S.; Skotland, T. The Protein Toxins Ricin and Shiga Toxin as Tools to Explore Cellular Mechanisms of Internalization and Intracellular Transport. *Toxins (Basel).* **2021**, *13* (6), 377.

(17) Liu, Y.; Tian, S.; Thaker, H.; Dong, M. Shiga Toxins: An Update on Host Factors and Biomedical Applications. *Toxins (Basel).* **2021**, *13* (3), 222.

(18) Liu, Z.; Li, X.; Lu, Z.; Qin, X.; Hong, H.; Zhou, Z.; Pieters, R. J.; Shi, J.; Wu, Z. *Repurposing the Pentameric B-Subunit of Shiga Toxin for Gb3-Targeted Immunotherapy of Colorectal Cancer by Rhamnose Conjugation.* **2022**, *111* (10), 2719−2729.

(19) Kostova, V.; Dransart, E.; Azoulay, M.; Brulle, L.; Bai, S. K.; Florent, J. C.; Johannes, L.; Schmidt, F. Targeted Shiga Toxin-Drug Conjugates Prepared via Cu-Free Click Chemistry. *Bioorg. Med. Chem.* **2015**, *23* (22), 7150−7157.

(20) Casas, M. G.; Stargardt, P.; Mairhofer, J.; Wiltschi, B. Decoupling Protein Production from Cell Growth Enhances the Site- Speci Fi c Incorporation of Noncanonical Amino Acids in E. Coli. *ACS Synth. Biol.* **2020**, *9* (11), 3052−3066.

(21) Danielewicz, N.; Dai, W.; Rosato, F.; Webb, M. E.; Striedner, G.; Römer, W.; Turnbull, W. B.; Mairhofer, J. In-Depth Characterization of a Re-Engineered Cholera Toxin Manufacturing Process Using Growth-Decoupled Production in Escherichia Coli. *Toxins (Basel).* **2022**, *14* (6), 396.

(22) Dorywalska, M.; Strop, P.; Melton-Witt, J. A.; Hasa-Moreno, A.; Farias, S. E.; Galindo Casas, M.; Delaria, K.; Lui, V.; Poulsen, K.; Loo, C.; Krimm, S.; Bolton, G.; Moine, L.; Dushin, R.; Tran, T. T.; Liu, S. H.; Rickert, M.; Foletti, D.; Shelton, D. L.; Pons, J.; Rajpal, A. Effect of Attachment Site on Stability of Cleavable Antibody Drug Conjugates. *Bioconjugate Chem.* **2015**, *26* (4), 650−659.

(23) Yoneda, Y.; Steiniger, S. C. J.; Capková, K.; Mee, J. M.; Liu, Y.; Kaufmann, G. F.; Janda, K. D. A Cell-Penetrating Peptidic GRP78 Ligand for Tumor Cell-Specific Prodrug Therapy. *Bioorg. Med. Chem. Lett.* **2008**, *18* (5), 1632−1636.

(24) Dubowchik, G. M.; Firestone, R. A.; Padilla, L.; Willner, D.; Hofstead, S. J.; Mosure, K.; Knipe, J. O.; Lasch, S. J.; Trail, P. A. Cathepsin B-Labile Dipeptide Linkers for Lysosomal Release of Doxorubicin from Internalizing Immunoconjugates: Model Studies of Enzymatic Drug Release and Antigen-Specific in Vitro Anticancer Activity. *Bioconjugate Chem.* **2002**, *13* (4), 855−869.

(25) Lee, M.-S.; Koo, S.; Jeong, D.; Tesh, V. Shiga Toxins as Multi-Functional Proteins : Induction of Host Cellular Stress Responses, Role in Pathogenesis and Therapeutic Applications. *Toxin* **2016**, *8* (3), 77.

(26) Zhao, R. Y.; Wilhelm, S. D.; Audette, C.; Jones, G.; Leece, B. A.; Lazar, A. C.; Goldmacher, V. S.; Singh, R.; Kovtun, Y.; Widdison, W. C.; Lambert, J. M.; Chari, R. V. J. Synthesis and Evaluation of Hydrophilic Linkers for Antibody-Maytansinoid Conjugates. *J. Med. Chem.* **2011**, *54* (10), 3606−3623.

(27) Pabst, M.; McDowell, W.; Manin, A.; Kyle, A.; Camper, N.; De Juan, E.; Parekh, V.; Rudge, F.; Makwana, H.; Kantner, T.; Parekh, H.; Michelet, A.; Sheng, X. B.; Popa, G.; Tucker, C.; Khayrzad, F.; Pollard, D.; Kozakowska, K.; Resende, R.; Jenkins, A.; Simoes, F.; Morris, D.; Williams, P.; Badescu, G.; Baker, M. P.; Bird, M.; Frigerio, M.; Godwin, A. Modulation of Drug-Linker Design to Enhance in Vivo Potency of Homogeneous Antibody-Drug Conjugates. *J. Controlled Release* **2017**, *253*, 160−164.

(28) Wang, Y.; Liu, L.; Fan, S.; Xiao, D.; Xie, F.; Li, W.; Zhong, W.; Zhou, X. Antibody-Drug Conjugate Using Ionized CYS-Linker-Mmae as the Potent Payload Shows Optimal Therapeutic Safety. *Cancers (Basel).* **2020**, *12* (3), 744.

(29) Bryant, P.; Pabst, M.; Badescu, G.; Bird, M.; McDowell, W.; Jamieson, E.; Swierkosz, J.; Jurlewicz, K.; Tommasi, R.; Henseleit, K.; Sheng, X.; Camper, N.; Manin, A.; Kozakowska, K.; Peciak, K.; Laurine, E.; Grygorash, R.; Kyle, A.; Morris, D.; Parekh, V.; Abhilash, A.; Choi, J. W.; Edwards, J.; Frigerio, M.; Baker, M. P.; Godwin, A. In Vitro and in Vivo Evaluation of Cysteine Rebridged Trastuzumab-MMAE Antibody Drug Conjugates with Defined Drug-to-Antibody Ratios. *Mol. Pharmaceutics* **2015**, *12* (6), 1872−1879.

(30) Dornan, D.; Bennett, F.; Chen, Y.; Dennis, M.; Eaton, D.; Elkins, K.; French, D.; Go, M. A. T.; Jack, A.; Junutula, J. R.; Koeppen, H.; Lau, J.; McBride, J.; Rawstron, A.; Shi, X.; Yu, N.; Yu, S. F.; Yue, P.; Zheng, B.; Ebens, A.; Polson, A. G. Therapeutic Potential of an Anti-CD79b Antibody-Drug Conjugate, Anti-CD79b-vc-MMAE, for the Treatment of Non-Hodgkin Lymphoma. *Blood* **2009**, *114* (13), 2721−2729.

https://doi.org/10.1021/acsomega.3c00667
ACS Omega 2023, 8, 15406−15421

(31) Koga, Y.; Manabe, S.; Aihara, Y.; Sato, R.; Tsumura, R.; Iwafuji, H.; Furuya, F.; Fuchigami, H.; Fujiwara, Y.; Hisada, Y.; Yamamoto, Y.; Yasunaga, M.; Matsumura, Y. Antitumor Effect of Antitissue Factor Antibody-MMAE Conjugate in Human Pancreatic Tumor Xenografts. *Int. J. Cancer* **2015**, *137* (6), 1457−1466.
(32) Mohseni, Z.; Sedighian, H.; Halabian, R.; Amani, J.; Behzadi, E.; Imani Fooladi, A. A. Potent in Vitro Antitumor Activity of B-Subunit of Shiga Toxin Conjugated to the Diphtheria Toxin against Breast Cancer. *Eur. J. Pharmacol.* **2021**, *899* (March), 174057.
(33) Simons, K.; Ikonen, E. Functional Rafts in Cell Membranes. *Nature* **1997**, *387* (6633), 569−572.
(34) Falguières, T.; Mallard, F.; Baron, C.; Hanau, D.; Lingwood, C.; Goud, B.; Salamero, J.; Johannes, L. Targeting of Shiga Toxin B-Subunit to Retrograde Transport Route in Association with Detergent-Resistant Membranes. *Mol. Biol. Cell* **2001**, *12* (8), 2453−2468.
(35) Schüller, S. Shiga Toxin Interaction with Human Intestinal Epithelium. *Toxins (Basel).* **2011**, *3* (6), 626−639.
(36) El Alaoui, A.; Schmidt, F.; Amessou, M.; Sarr, M.; Decaudin, D.; Florent, J. C.; Johannes, L. Shiga Toxin-Mediated Retrograde Delivery of a Topoisomerase I Inhibitor Prodrug. *Angew. Chemie - Int. Ed.* **2007**, *46* (34), 6469−6472.
(37) Mellor, G. E.; Goulter, R. M.; Chia, T. W. R.; Dykes, G. A. Comparative Analysis of Attachment of Shiga-Toxigenic Escherichia Coli and Salmonella Strains to Cultured HT-29 and Caco-2 Cell Lines. *Appl. Environ. Microbiol.* **2009**, *75* (6), 1796−1799.
(38) Kirn, T. J.; Jude, B. A.; Taylor, R. K. A Colonization Factor Links Vibrio Cholerae Environmental Survival and Human Infection. *Nature* **2005**, *438* (7069), 863−866.
(39) Pinho, S. S.; Reis, C. A. Glycosylation in Cancer: Mechanisms and Clinical Implications. *Nat. Rev. Cancer* **2015**, *15* (9), 540−555.
(40) Celi, A. B.; Goldstein, J.; Rosato-Siri, M. V.; Pinto, A. Role of Globotriaosylceramide in Physiology and Pathology. *Front. Mol. Biosci.* **2022**, *9*, 20.
(41) Batisse, C.; Dransart, E.; Ait Sarkouh, R.; Brulle, L.; Bai, S. K.; Godefroy, S.; Johannes, L.; Schmidt, F. A New Delivery System for Auristatin in STxB-Drug Conjugate Therapy. *Eur. J. Med. Chem.* **2015**, *95*, 483−491.
(42) Melendez, A. V.; Velasco Cardenas, R. M.-H.; Lagies, S.; Strietz, J.; Siukstaite, L.; Thomas, O. S.; Tomisch, J.; Weber, W.; Kammerer, B.; Romer, W.; Minguet, S. Novel Lectin - Based Chimeric Antigen Receptors Target Gb3 - Positive Tumour Cells. *Cell. Mol. Life Sci.* **2022**, *79* (10), 1−25.
(43) Stargardt, P.; Striedner, G.; Mairhofer, J. Tunable Expression Rate Control of a Growth-Decoupled T7 Expression System by l-Arabinose Only. *Microb. Cell Fact.* **2021**, *20* (1), 1−17.
(44) Rosato, F.; Pasupuleti, R.; Tomisch, J.; Meléndez, A. V.; Kolanovic, D.; Makshakova, O. N.; Wiltschi, B.; Römer, W. A Bispecic, Crosslinking Lectibody Activates Cytotoxic T Cells and Induces Cancer Cell Death. *J. Transl. Med.* **2022**, *20*, 1−26.
(45) Galindo Casas, M.; Stargardt, P.; Mairhofer, J.; Wiltschi, B. Decoupling Protein Production from Cell Growth Enhances the Site-Specific Incorporation of Noncanonical Amino Acids in E. Coli. *ACS Synth. Biol.* **2020**, *9* (11), 3052−3066.
(46) Abe, A.; Inokuchi, J.-i.; Jimbo, M.; Shimeno, H.; Nagamatsu, A.; Shayman, J. A.; Shukla, G. S.; Radin, N. S. Improved Inhibitors of Glucosylceramide Synthase. *J. Biol. Chem.* **1992**, *111* (2), 191−196.
(47) Gallegos, K. M.; Conrady, D. G.; Karve, S. S.; Gunasekera, T. S.; Herr, A. B.; Weiss, A. A. Shiga Toxin Binding to Glycolipids and Glycans. *PLoS One* **2012**, *7* (2), No. e30368.
(48) Stargardt, P.; Feuchtenhofer, L.; Cserjan-Puschmann, M.; Striedner, G.; Mairhofer, J. Bacteriophage Inspired Growth-Decoupled Recombinant Protein Production in Escherichia Coli. *ACS Synth. Biol.* **2020**, *9* (6), 1336−1348.
(49) Felinger, A.; Pasti, L.; Dondi, F.; Van Hulst, M.; Schoenmakers, P. J.; Martin, M. Stochastic Theory of Size Exclusion Chromatography: Peak Shape Analysis on Single Columns. *Anal. Chem.* **2005**, *77* (10), 3138−3148.
(50) Xu, J.; Zhao, W.; Sun, J.; Huang, Y.; Wang, P.; Venkataramanan, R.; Yang, D.; Ma, X.; Rana, A.; Li, S. Novel Glucosylceramide Synthase Inhibitor Based Prodrug Copolymer Micelles for Delivery of Anticancer Agents. *J. Controlled Release* **2018**, *288*, 212−226.
(51) McMillin, D. W.; Delmore, J.; Negri, J. M.; Vanneman, M.; Koyama, S.; Schlossman, R. L.; Munshi, N. C.; Laubach, J.; Richardson, P. G.; Dranoff, G.; Anderson, K. C.; Mitsiades, C. S. Compartment-Specific Bioluminescence Imaging Platform for the High-Throughput Evaluation of Antitumor Immune Function. *Blood* **2012**, *119* (15), 131−138.
(52) McMillin, D. W.; Delmore, J.; Weisberg, E.; Negri, J. M.; Geer, D. C.; Klippel, S.; Mitsiades, N.; Schlossman, R. L.; Munshi, N. C.; Kung, A. L.; Griffin, J. D.; Richardson, P. G.; Anderson, K. C.; Mitsiades, C. S. Tumor Cell-Specific Bioluminescence Platform to Identify Stroma-Induced Changes to Anticancer Drug Activity. *Nat. Med.* **2010**, *16* (4), 483−489.
(53) Nudelman, E.; Kannagi, R.; Hakomori, S.; Parsons, M.; Lipinski, M.; Wiels, J.; Fellous, M.; Tursz, T. A Glycolipid Antigen Associated with Burkitt Lymphoma Defined by a Monoclonal Antibody. *Science (80-.).* **1983**, *220* (4596), 509−511.
(54) Johansson, D.; Kosovac, E.; Moharer, J.; Ljuslinder, I.; Brännström, T.; Johansson, A.; Behnam-Motlagh, P. Expression of Verotoxin-1 Receptor Gb3 in Breast Cancer Tissue and Verotoxin-1 Signal Transduction to Apoptosis. *BMC Cancer* **2009**, *9*, 1−9.
(55) LaCasse, E. C.; Bray, M. R.; Patterson, B.; Lim, W. M.; Perampalam, S.; Radvanyi, L. G.; Keating, A.; Stewart, A. K.; Buckstein, R.; Sandhu, J. S.; Miller, N.; Banerjee, D.; Singh, D.; Belch, A. R.; Pilarski, L. M.; Gariépy, J. Shiga-like Toxin-1 Receptor on Human Breast Cancer, Lymphoma, and Myeloma and Absence from CD34+ Hematopoietic Stem Cells: Implications for Ex Vivo Tumor Purging and Autologous Stem Cell Transplantation. *Blood* **1999**, *94* (8), 2901−2910.
(56) Arab, S.; Russel, E.; Chapman, W. B.; Rosen, B.; Lingwood, C. A. Expression of the Verotoxin Receptor Glycolipid, Globotriaosylceramide, in Ovarian Hyperplasias. *Oncol. Res.* **1997**, *9* (10), 553−563.
(57) Maak, M.; Nitsche, U.; Keller, L.; Wolf, P.; Sarr, M.; Thiebaud, M.; Rosenberg, R.; Langer, R.; Kleeff, J.; Friess, H.; Johannes, L.; Janssen, K. P. Tumor-Specific Targeting of Pancreatic Cancer with Shiga Toxin B-Subunit. *Mol. Cancer Ther.* **2011**, *10* (10), 1918−1928.
(58) Geyer, P. E.; Maak, M.; Nitsche, U.; Perl, M.; Novotny, A.; Slotta-Huspenina, J.; Dransart, E.; Holtorf, A.; Johannes, L.; Janssen, K. P. Gastric Adenocarcinomas Express the Glycosphingolipid Gb3/CD77: Targeting of Gastric Cancer Cells with Shiga Toxin B-Subunit. *Mol. Cancer Ther.* **2016**, *15* (5), 1008−1017.
(59) Schubert, T.; Sych, T.; Madl, J.; Xu, M.; Omidvar, R.; Patalag, L. J.; Ries, A.; Kettelhoit, K.; Brandel, A.; Mely, Y.; Steinem, C.; Werz, D. B.; Thuenauer, R.; Römer, W. Differential Recognition of Lipid Domains by Two Gb3-Binding Lectins. *Sci. Rep.* **2020**, *10* (1), 1−12.
(60) Pellizzari, A.; Pang, H.; Lingwood, C. A. Binding of Verocytotoxin 1 to Its Receptor Is Influenced by Differences in Receptor Fatty Acid Content. *Biochemistry* **1992**, *31* (5), 1363−1370.
(61) Binnington, B.; Lingwood, D.; Nutikka, A.; Lingwood, C. A. Effect of Globotriaosyl Ceramide Fatty Acid α-Hydroxylation on the Binding by Verotoxin 1 and Verotoxin 2. *Neurochem. Res.* **2002**, *27* (7−8), 807−813.
(62) Siukstaite, L.; Imberty, A.; Römer, W. Structural Diversities of Lectins Binding to the Glycosphingolipid Gb3. *Front. Mol. Biosci.* **2021**, *8* (July), 1−16.
(63) Viel, T.; Dransart, E.; Nemati, F.; Henry, E.; Theze, B.; Decaudin, D.; Lewandowski, D.; Boisgard, R.; Johannes, L.; Tavitian, B. In Vivo Tumor Targeting by the B-Subunit of Shiga Toxin. *Mol. Imaging* **2008**, *7* (6), 239−247.
(64) Janssen, K.-P.; Vignjevic, D.; Boisgard, R.; Falguieres, T.; Bousquet, G.; Decaudin, D.; Dolle, F.; Louvard, D.; Tavitian, B.; Robine, S.; Johannes, L. In Vivo Tumor Targeting Using a Novel Intestinal Pathogen-Based Delivery Approach. *Cancer Res.* **2006**, *66* (14), 7230−7236.

https://doi.org/10.1021/acsomega.3c00667
ACS Omega 2023, 8, 15406−15421

(65) Mazor, R.; King, E. M.; Pastan, I. Strategies to Reduce the Immunogenicity of Recombinant Immunotoxins. *Am. J. Pathol.* **2018**, *188* (8), 1736−1743.
(66) Sandvig, K. NEW EMBO MEMBERS' REVIEW: Entry of Ricin and Shiga Toxin into Cells: Molecular Mechanisms and Medical Perspectives. *EMBO J.* **2000**, *19* (22), 5943−5950.
(67) Sandvig, K. Shiga Toxins. *Toxicon* **2001**, *39* (11), 1629−1635.
(68) Vingert, B.; Adotevi, O.; Patin, D.; Jung, S.; Shrikant, P.; Freyburger, L.; Eppolito, C.; Sapoznikov, A.; Amessou, M.; Quintin-Colonna, F.; Fridman, W. H.; Johannes, L.; Tartour, E. The Shiga Toxin B-Subunit Targets Antigen in Vivo to Dendritic Cells and Elicits Anti-Tumor Immunity. *Eur. J. Immunol.* **2006**, *36* (5), 1124−1135.
(69) Center for Drug Evaluation and Research (no date) Guidance for industry. *U.S. Food and Drug Administration. FDA*. Available at: https://www.fda.gov/regulatory-information/search-fda-guidance-documents/immunogenicity-testing-therapeutic-protein-products-developing-and-validating-assays-anti-drug (Accessed: March 2, 2023).
(70) Gribben, J. G.; Devereux, S.; Thomas, N. S. B.; Keim, M.; Jones, H. M.; Goldstone, A. H.; Linch, D. C. Development of antibodies to unprotected glycosylation sites on recombinant human GM-CSF. *Lancet.* **1990**, *335* (8687), 434−437.
(71) Hwang, W. Y. K.; Foote, J. *Immun. Eng. Antibod. Methods.* **2005**, *36* (1), 3−10.
(72) Cioci, G.; Mitchell, E. P.; Gautier, C.; Wimmerová, M.; Sudakevitz, D.; Pérez, S.; Gilboa-Garber, N.; Imberty, A. Structural Basis of Calcium and Galactose Recognition by the Lectin PA-IL of Pseudomonas Aeruginosa. *FEBS Lett.* **2003**, *555* (2), 297−301.

https://doi.org/10.1021/acsomega.3c00667
ACS Omega 2023, 8, 15406−15421